Semiconductor Science and Technology

Magneto-optical properties of semimagnetic lead chalcogenides

Semicond. Sci. Technol. 7 (1992) 703–723. Printed in the UK

REVIEW ARTICLE

Magneto-optical properties of semimagnetic lead chalcogenides

Günther Bauer†, Harald Pascher‡ and Wlodek Zawadzki§

† Institut für Halbleiterphysik, Johannes Kepler Universität Linz, A-4040 Linz, Austria
‡ Experimentalphysik I, Universität Bayreuth, D-8580 Bayreuth, Federal Republic of Germany
§ Institute of Physics, Polish Academy of Sciences, PL-02 668 Warszawa, Poland

Received 21 February 1992, accepted for publication 9 March 1992

Abstract. Magneto-optical properties of PbTe and PbSe alloyed with paramagnetic ions Mn and Eu are reviewed. The $\boldsymbol{k}\cdot\boldsymbol{p}$ theory of the band structure of IV–VI compounds is presented, taking into account the narrow energy gaps and strong spin–orbit interactions in the materials. The exchange interaction between the paramagnetic ions and mobile carriers is included in the framework of the mean-field approximation. The experimental data of various authors on magnetization, interband magneto-optics, intraband magneto-optics and four-wave mixing are presented. All results are successfully described by the theory, treating the exchange integrals as adjustable parameters. It is shown that the exchange interaction is of particular importance for the valence bands. Differences between semimagnetic behaviours of Mn-based and Eu-based systems are emphasized as well as those between the IV–VI and II–VI semimagnetic compounds.

1. Introduction

Lead salt IV–VI compounds PbTe, PbSe, PbS belong to the oldest known semiconducting materials. They have been intensively investigated in view of their interesting physical properties: strong temperature dependences of energy gaps, very high dielectric constants, soft phonon modes, displacive phase transitions, etc. They have been also studied as materials for optical detectors and semiconductor lasers in the infrared spectral range. The lead salts are characterized by a rather complicated energy band structure. The band extrema occur at the L points of the Brillouin zone, which results in non-sphericity of the bands and a multivalley structure of both conduction and valence bands. In addition, the small values of energy gaps lead to a strong $\boldsymbol{k}\cdot\boldsymbol{p}$ interaction which in turn results in pronounced non-parabolicity of the $E(k)$ dispersion relations. The classical properties of lead salts and their alloys, most notably with Sn, have been reviewed in many publications (e.g. Ravich *et al* 1970, Dalven 1973). The small energy gaps lead to small effective masses of electrons and holes. On the other hand the strong spin–orbit interaction (Pb is a heavy element) leads to large values of the spin-splitting g-factors. All this results in pronounced Landau and spin quantization of the energy spectrum at available magnetic fields.

It has been known for some years that paramagnetic ions like Mn^{2+}, Cr^{2+} and Fe^{2+} strongly influence the properties of mobile electrons and holes in II–VI compounds: HgTe, HgSe, CdTe, CdSe, etc (Furdyna 1988, Furdyna and Kossut 1988). In the presence of an external magnetic field, the paramagnetic ions become partially aligned along the field, which results in an additional internal magnetization of the material. This magnetization strongly influences the spin properties of mobile carriers, while the orbital properties are influenced in the usual way via the change of energy gap and the resulting effective masses. At high magnetic fields, the magnetization of paramagnetic ions saturates and their influence becomes less dramatic. The effect of paramagnetic ions on mobile carriers is usually described within the framework of a mean-field theory for the exchange interaction between the ion and the carrier magnetic moments (Galazka and Kossut 1980). It turned out that the paramagnetic ions also have a strong effect on mobile holes in lead salt IV–VI compounds (Pascher *et al* 1989). On the other hand the effect on the electrons is much weaker than in the II–VI compounds.

The present paper reviews magneto-optical investigations of semimagnetic IV–VI compounds (called also diluted magnetic semiconductors). We concentrate on optical studies since magnetotransport studies are

0268-1242/92/060703+21 $04.50

usually not conclusive in the band structure investigations. The reason is that the magnetotransport effects oscillate whenever the Fermi level crosses a magnetic level. However, the position of the Fermi level is itself determined by the band structure, so that the conclusions based on transport experiments are often 'self-fulfilling prophecies'. On the other hand, the optical experiments dispose of an energy standard given by the photon frequency. In addition, one can use the light polarization and various magneto-optical configurations in order to influence the selection rules of optical transitions. This provides a powerful tool for physical interpretation. As a result, optical experiments, described using an adequate theory, provide conclusive insight into the material properties.

The paper is organized in the following way: in section 2 we present a theoretical description of the band structure of 'classical' lead salts PbTe, PbSe and PbS and the influence of paramagnetic ions on mobile carriers. Section 3 enumerates experimental methods and briefly indicates what information can be obtained from various studies. In section 3.1 we show the results of magnetization experiments (to the extent necessary for an understanding of the optical data). Section 3.2 discusses the interband magneto-optics, section 3.3 the intraband magneto-optics and section 3.4 the four-wave mixing results; this section gives direct information on the spin g-values which are particularly useful in the studies of semimagnetic materials. In the conclusion we discuss the difference between Mn- and Eu-based alloys and mention subjects demanding further clarification.

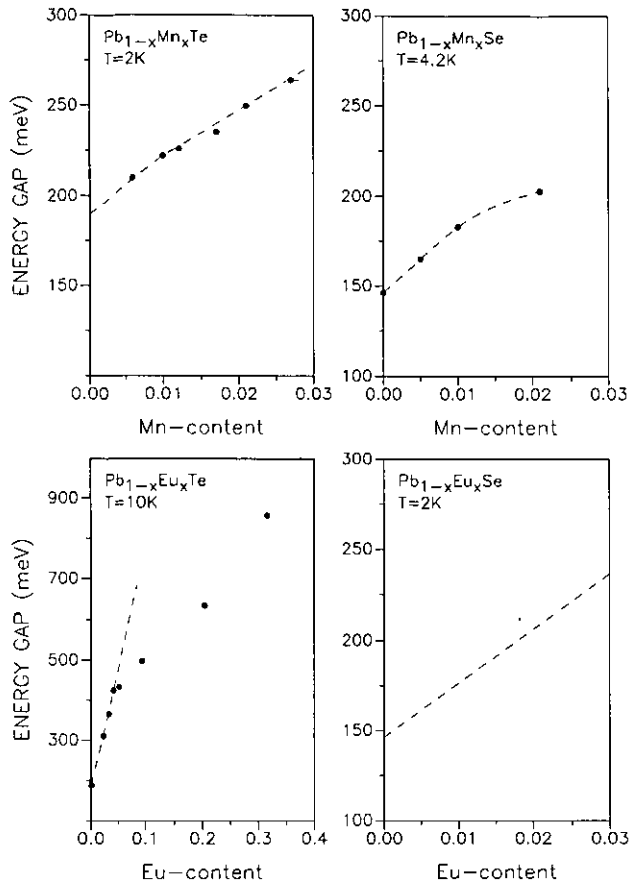

Figure 1. Dependence of the energy gap on composition for four compounds: $Pb_{1-x}Mn_xTe$ (Pascher and Bauer 1987); $Pb_{1-x}Mn_xSe$ (Kowalczyk 1991); $Pb_{1-x}Eu_xTe$ (Partin 1988); and $Pb_{1-x}Eu_xSe$ (Lambrecht *et al* 1991).

2. Theory

For comparatively small concentrations of the magnetic ions the IV–VI compounds have a direct narrow energy gap (figure 1) at the L point of the Brillouin zone. The electron and hole masses are more or less mirror images of each other, the mass anisotropies $K = m_l/m_t$ vary from 10 (PbTe) to about 2 (PbSe). In figure 2 the surfaces of constant energy are shown with their axes oriented along the $\langle 111 \rangle$ directions for three orientations of an external magnetic field. The symbol ϕ denotes the angle between main axes of the ellipsoids and the magnetic field.

The theoretical section consists of two parts. In section 2.1 we briefly describe conduction and valence bands of IV–VI lead chalcogenides in the presence of an external magnetic field. Section 2.2 is concerned with magnetic ions and their effect on the Landau and spin levels. These results are necessary for the description of experimental data presented later.

2.1. Landau and spin levels in lead chalcogenides near band extrema

Our treatment is based on the $k \cdot p$ theory of the band structure, in which the lowest conduction and highest valence bands are included exactly, while two higher conduction and two lower valence bands are taken into account in approximation to k^2 terms. Our description follows Mitchell and Wallis (1966), Dimmock (1971), Adler *et al* (1973), Burkhard *et al* (1979) and Bernick and Kleinman (1970), correcting mistakes, inconsistencies and misprints, when necessary.

The initial eigenvalue problem for the semiconductor electron in the presence of an external magnetic field reads

$$\left(\frac{1}{2m_0}P^2 + V_0(r) + H_{so}\right)\psi = E\psi \qquad (1)$$

where V_0 is the periodic potential of the lattice, H_{so} is the spin–orbit interaction, $\boldsymbol{P} = \boldsymbol{p} + e\boldsymbol{A}$ is the kinetic momentum, and $\boldsymbol{A}$ is the vector potential of magnetic field. Due to the presence of magnetic field, the Hamiltonian in equation (1) is not periodic. One looks for the solutions in the form

$$\psi = \sum_l f_l(r)u_l(r) \qquad (2)$$

where f_l are envelope (slowly varying) functions, while $u_l(r)$ are periodic Luttinger–Kohn (L–K) functions at the band extrema (the L point in our case). The summation is over the energy bands. The L–K functions satisfy the eigenvalue problems at the band edges

$$\left(\frac{1}{2m_0}P^2 + V_0(r) + H_{so}\right)u_l = \varepsilon_{l0}u_l. \qquad (3)$$

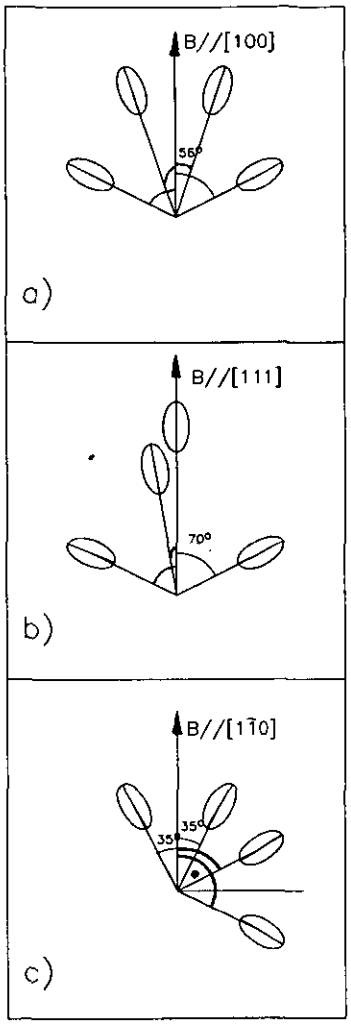

Figure 2. Orientation of main ellipsoid axes with respect to applied magnetic field for three principal field directions. (*a*) $\boldsymbol{B} \parallel [100]$: four valleys are equivalent to each other ($\phi = 56.34°$). (*b*) $\boldsymbol{B} \parallel [111]$. Two sets of valleys have to be distinguished: one valley is oriented with its main axes parallel to $\boldsymbol{B}(\phi \approx 0°)$, three valleys are oriented obliquely to $\boldsymbol{B}(\phi = 70.53°)$. (*c*) $\boldsymbol{B} \parallel [1\bar{1}0]$ the main axes of two valleys are oriented by $\phi = 35.26°$, the two other ones with $\phi = 90°$ with respect to $\boldsymbol{B}$.

One inserts the functions (2) into equation (1), multiplies on the left by $u_l^*(\boldsymbol{r})$ and integrates over the unit cell. Making use of the orthogonality of the L-K functions the initial problem (1) is transformed into

$$\sum_l H_{l'l} f_l = E f_{l'} \qquad l' = 1,2,\ldots \tag{4}$$

where l' runs over energy bands. The $\boldsymbol{P} \cdot \boldsymbol{\pi}$ Hamiltonian, written to the second order in $\boldsymbol{P}$ operators, is

$$H_{l'l} = \left(\varepsilon_{l0} + \frac{1}{2m_0} P^2\right)\delta_{l'l} + \frac{1}{m_0^2} \sum_{\alpha\beta=1}^{3} A_{l'l}^{\alpha\beta} P_\alpha P_\beta + \frac{1}{m_0} \boldsymbol{\pi}_{l'l} \cdot \boldsymbol{P} + \mu_B \boldsymbol{B} \cdot \boldsymbol{\sigma}_{l'l} \tag{5}$$

where l' and l are band indices, α and β are cartesian coordinates, ε_{l0} are band-edge energies, $\boldsymbol{\pi}_{l'l} = \langle u_{l'} | \boldsymbol{\pi} | u_l \rangle$ are matrix elements of

$$\boldsymbol{\pi} = \boldsymbol{p} + \frac{\hbar}{4m_0c^2}(\boldsymbol{\sigma} \times \nabla V_0) \tag{6}$$

and $\sigma_{l'l} = \langle u_{l'} | \boldsymbol{\sigma} | u_l \rangle$, where $\boldsymbol{\sigma}$ are the Pauli spin operators; μ_B is the Bohr magneton. In the diagonal elements of $\boldsymbol{\pi}_{l'l}$ the contribution of spin-orbit interaction disappears (cf Bir and Pikus 1974), while in the non-diagonal elements it is very small compared with the $\boldsymbol{p}$ contribution.

The coefficients in front of quadratic P terms in the Hamiltonian (equation (5)) are

$$A_{l'l}^{\alpha\beta} = \sum_{l''} \frac{\boldsymbol{\pi}_{l'l''}^{\alpha} \cdot \boldsymbol{\pi}_{l''l}^{\beta}}{\varepsilon_{l'0} - \varepsilon_{l''0}}. \tag{7}$$

In general different components of $\boldsymbol{P}$ do not commute. As a consequence, the symmetric components of $A_{l'l}^{\alpha\beta}$ contribute to the orbital magnetic terms of P^2 form, while the antisymmetric terms contribute to the spin splitting (cf Zeiger and Pratt 1973).

The band-edge periodic functions for the valence ($V^{\pm}$) bands at the L-point of the Brillouin zone have the L_{61}^{+} symmetry. They are given (in the Mitchell and Wallis notation) by

$$\begin{aligned} V^{+} &= i \cos\theta^{+} R\uparrow + \sin\theta^{+} S_{+}\downarrow \\ V^{-} &= i \cos\theta^{+} R\downarrow + \sin\theta^{+} S_{-}\uparrow . \end{aligned} \tag{8}$$

On the other hand, the bandedge conduction states in PbTe and PbSe have different symmetries. According to Bernick and Kleinman (1970) (cf also Martinez *et al* 1975) the band-edge symmetry of the conduction band is L_{63}^{-} (or L_{62}^{-} in the Mitchell and Wallis notation):

$$\begin{aligned} C^{+} &= -\sin\theta^{-} Z\uparrow - \cos\theta^{-} X_{+}\downarrow \\ C^{-} &= \sin\theta^{-} Z\downarrow - \cos\theta^{-} X_{-}\uparrow . \end{aligned} \tag{9}$$

The band-edge symmetry of the conduction band in PbSe is L_{62}^{-} in Bernick and Kleinman and L_{61}^{-} in Mitchell-Wallis notations:

$$\begin{aligned} C^{+} &= -\cos\theta^{-} Z\uparrow + \sin\theta^{-} X_{+}\downarrow \\ C^{-} &= \cos\theta^{-} Z\downarrow + \sin\theta^{-} X_{-}\uparrow . \end{aligned} \tag{10}$$

The parameters $\cos\theta^{\pm}$ and $\sin\theta^{\pm}$ are given by different combinations of energy gaps and spin-orbit energies (cf Mitchell and Wallis 1966). The different symmetries of the conduction band states in PbTe and PbSe explain the large difference in the anistropy of their conduction bands (cf Bernick and Kleinman 1970).

The + and − superscripts denote the partners of a Kramers pair, and they do not correspond to pure spin states. The spin functions $\uparrow$ and $\downarrow$ refer to eigenstates of σ_z in the atomic coordinate system with z along the [111] axis of the valley, x along $[\bar{1}\bar{1}2]$ and y along $[1\bar{1}0]$. The spatial parts of the wavefunctions have the following transformation properties about the site of the metal nucleons: R is isotropic (atomic s state), $X_{\pm}$ and Z

transform like the atomic p functions with $m_z = \pm 1$ and $m_Z = 0$, respectively, and $S_\pm$ transform like the atomic d functions with $m_z = \pm 1$. The spin-orbit mixing parameters cos $\theta^\pm$ are obtained from the band-structure calculations. The higher and lower bands are described by similar expressions. The $\boldsymbol{P}\cdot\boldsymbol{\pi}$ terms of the four band-edge states are

$$\begin{aligned}
&\frac{1}{m_0}\langle V^+|\pi|C^+\rangle\cdot\boldsymbol{P} = v_l P_z \\
&\frac{1}{m_0}\langle V^+|\pi|C^-\rangle\cdot\boldsymbol{P} = \sqrt{2}v_t P_- \\
&\frac{1}{m_0}\langle V^-|\pi|C^+\rangle\cdot\boldsymbol{P} = \sqrt{2}v_t P_+ \\
&\frac{1}{m_0}\langle V^-|\pi|C^-\rangle\cdot\boldsymbol{P} = -v_l P_z
\end{aligned} \tag{11}$$

where $P\pm = (P_x \pm iP_y)/\sqrt{2}$, while v_l and v_t are appropriate combinations of matrix elements and cos $\theta^\pm$, sin $\theta^\pm$ (cf Mitchell and Wallis 1966, Adler *et al* 1973). Similarly one calculates the matrix elements including two upper conduction and two lower valence bands appearing in equation (7). As a result, the eigenvalue problem for the envelope functions f_l,

$$\sum_{l=1}^{4} H_{l'l} f_l = E f_{l'} \qquad l' = 1, \ldots, 4 \tag{12}$$

is described by the following Hamiltonian. The zero of energy is chosen at the middle of energy gap, the ordering is clear from the diagonal terms

$$\begin{bmatrix}
\hat{V}^+ & \frac{1}{2}g_t^+\mu_B B_x & v_l P_z & \sqrt{2}v_t P_- \\
\frac{1}{2}g_t^+\mu_B B_x & \hat{V}^- & \sqrt{2}v_t P_+ & -v_l P_z \\
v_l P_z & \sqrt{2}v_t P_- & \hat{C}^+ & \frac{1}{2}g_t^-\mu_B B_x \\
\sqrt{2}v_t P_+ & -v_l P_z & \frac{1}{2}g_t^-\mu_B B_x & \hat{C}^-
\end{bmatrix} \tag{13}$$

where

$$\hat{V}^\pm = \frac{-E_g}{2} - \frac{P_x^2 + P_y^2}{2m_t^+} - \frac{P_z^2}{2m_l^+} \pm \frac{1}{2}g_l^+\mu_B B_z \tag{14}$$

$$\hat{C}^\pm = \frac{+E_g}{2} + \frac{P_x^2 + P_y^2}{2m_t^-} + \frac{P_z^2}{2m_l^-} \pm \frac{1}{2}g_l^-\mu_B B_z \tag{15}$$

in which $m_t^\pm$, $m_l^\pm$, $g_t^\pm$, $g_l^\pm$ denote far-band contributions to the effective masses and the spin g-values, respectively. Plus and minus superscripts refer traditionally to the valence and the conduction band, respectively.

Thus the eigenvalue problem (equation (12)) presents a set of four coupled differential equations. If the magnetic field is directed along the [111] crystal direction, i.e. $\boldsymbol{B} = (0, 0, B)$ in the above chosen coordinate system, the set (equation (13)) can be solved in terms of harmonic oscillator functions. Choosing the Landau gauge for the vector potential $\boldsymbol{A} = [0, Bx, 0]$, the following relations are satisfied

$$\begin{aligned}
P_+|n\rangle &= -(\hbar/L)\sqrt{(n+1)}|n+1\rangle \\
P_-|n\rangle &= -(\hbar/L)\sqrt{n}|n-1\rangle \\
P_z \exp(ik_z z) &= \hbar k_z \exp(ik_z z)
\end{aligned} \tag{16}$$

where

$$|n\rangle = i^n \exp(ik_y y)\Phi_n\left(\frac{x - x_0}{L}\right) \tag{17}$$

in which $L = (\hbar c/eB)^{1/2}$ is the magnetic radius, $x_0 = k_y L^2$, and Φ_n is the normalized harmonic oscillator function. It can then be checked by inspection that the wavefunction

$$\psi_n = \exp(ik_z z)\begin{bmatrix} \alpha_1|n\rangle \\ \alpha_2|n+1\rangle \\ \alpha_3|n\rangle \\ \alpha_4|n+1\rangle \end{bmatrix} \tag{18}$$

satisfies the set of equations (12). Upon acting with the above function the differential set for f_l becomes a set of linear equations for α_l, which can be solved for the eigenvalues E. For the case $k_z = 0$, which is of experimental interest, the 4×4 set decouples into two 2×2 sets, which can be solved analytically. The result is (cf Burkhard *et al* 1979)

$$E_{v,n,-}^{c,n,+} = \tfrac{1}{2}(\tilde{a}_n + \tilde{b}_n) \pm \tfrac{1}{2}[(\tilde{a}_n - \tilde{b}_n)^2 + 4E_g\hbar\omega_{cv}(n+1)]^{1/2} \tag{19}$$

$$E_{v,n,+}^{c,n,-} = \tfrac{1}{2}(\tilde{c}_n + \tilde{d}_n) \pm \tfrac{1}{2}[(\tilde{c}_n - \tilde{d}_n)^2 + 4E_g\hbar\omega_{cv}(n+1)]^{1/2} \tag{20}$$

where

$$\begin{aligned}
\tilde{a}_n &= +\tfrac{1}{2}E_g + \hbar\omega_l^-(n+\tfrac{1}{2}) + \tfrac{1}{2}g_l^-\mu_B B \\
\tilde{b}_n &= -\tfrac{1}{2}E_g + \hbar\omega_l^+(n+\tfrac{3}{2}) - \tfrac{1}{2}g_l^+\mu_B B \\
\tilde{c}_n &= +\tfrac{1}{2}E_g + \hbar\omega_l^-(n+\tfrac{3}{2}) - \tfrac{1}{2}g_l^-\mu_B B \\
\tilde{d}_n &= -\tfrac{1}{2}E_g + \hbar\omega_l^+(n+\tfrac{1}{2}) + \tfrac{1}{2}g_l^+\mu_B B
\end{aligned} \tag{21}$$

The dominant cyclotron frequency is $\omega_{cv} = eB/m_{cv}c$, with $m_{cv} = E_g/2v_t^2$. The quantity m_{cv} is the main contribution to the effective mass coming from the valence-conduction two-band interaction. The cyclotron frequencies $\omega_l^\pm = eB/m_l^\pm c$ come from far-band contributions.

The Landau quantum number in equations (19)-(21) takes the values $n = 0, 1, 2, \ldots$. However, the highest valence and the lowest conduction Landau levels are: $E_{v,-1,-} = \tilde{b}_{-1}$ and $E_{c,-1,-} = \tilde{c}_{-1}$. As seen from equations (19)-(21) these energies are linear in magnetic field. In general, however, the Landau energies, given by equations (19)-(21) are sublinear in B. This is an effect of band non-parabolicity, resulting from the small value of the energy gap E_g. The far-band terms lift degeneracy of $|n, +\rangle$ and $|n+1, -\rangle$ states. In the following we use a more physical notation, increasing the n numbers of the $|-\rangle$ states in both bands by one and ascribing an effective spin $s = \pm 1/2$ to the $|\pm\rangle$ states.

The isoenergetic surfaces resulting from the above

band model (two levels taken into account exactly and four levels included in the k^2 approximation) are approximately ellipsoidal. They would have been perfect ellipsoids of revolution (around the [111] and equivalent crystal directions) had the far-band contributions to the effective masses satisfied the relations

$$\frac{m_l^-}{m_t^-} = \frac{m_l^+}{m_t^+} = \frac{v_t^2}{v_l^2}. \tag{22}$$

This is in general not the case. Nevertheless, the experimental experience indicates that the non-ellipsoidal constant-energy surfaces are practically indistinguishable from ellipsoids up to quite high electron and hole energies. Such energies are usually not reached in magneto-optical experiments and are rarely reached in transport experiments (for samples with free-carrier concentrations above $5 \times 10^{19}\,\mathrm{cm}^{-3}$). Thus, it will be assumed in the following that equations (22) are satisfied, even if the finally determined band parameters slightly disobey them. We discuss this point somewhat later.

If the constant-energy surfaces are ellipsoidal, it is possible to solve the eigenvalue problem for arbitrary direction of magnetic field (cf Lax and Mavroides 1960, Adler *et al* 1973). One applies a two-step coordinate transformation, the first step being a scale change according to relative sizes of v_t and v_l, the second step being a rotation to align the z axis of the final coordinate system with the direction of the magnetic field. Let a magnetic field have direction cosines λ_x and λ_z in the x, z plane. The two-step transformation is equivalent to performing the unitary transformation on the Hamiltonian of equation (13)

$$\hat{\mathbf{H}} = \mathbf{T}^{-1}\,\mathbf{H}\mathbf{T} \tag{23}$$

where

$$\mathbf{T} = \begin{pmatrix} \cos\frac{1}{2}\gamma & -\sin\frac{1}{2}\gamma & 0 & 0 \\ \sin\frac{1}{2}\gamma & \cos\frac{1}{2}\gamma & 0 & 0 \\ 0 & 0 & \cos\frac{1}{2}\gamma & -\sin\frac{1}{2}\gamma \\ 0 & 0 & \sin\frac{1}{2}\gamma & \cos\frac{1}{2}\gamma \end{pmatrix} \tag{24}$$

in which $\sin\gamma = \lambda_x v_l v_t / v_B^2$ and

$$v_B^2 = v_t\sqrt{\lambda_z^2 v_t^2 + \lambda_x^2 v_l^2}. \tag{25}$$

The transformed Hamiltonian is

$$\begin{bmatrix} \hat{\tilde{V}}^+ & \frac{1}{2}\tilde{g}_t^+\mu_B B & \left(\frac{E_g}{2m_B}\right)^{1/2} P_B & (E_g\hbar\tilde{\omega}_c)^{1/2}\Lambda_- \\ \frac{1}{2}\tilde{g}_t^+\mu_B B & \hat{\tilde{V}}^- & (E_g\hbar\tilde{\omega}_c)^{1/2}\Lambda_+ & -\left(\frac{E_g}{2m_B}\right)^{1/2} P_B \\ \left(\frac{E_g}{2m_B}\right)^{1/2} P_B & (E_g\hbar\tilde{\omega}_c)^{1/2}\Lambda_- & \hat{\tilde{C}}^+ & \frac{1}{2}\tilde{g}_t^-\mu_B B \\ (E_g\hbar\tilde{\omega}_c)^{1/2}\Lambda_+ & -\left(\frac{E_g}{2m_B}\right)^{1/2} P_B & \frac{1}{2}\tilde{g}_t^-\mu_B B & \hat{\tilde{C}}^- \end{bmatrix} \tag{26}$$

where

$$\begin{aligned} \tilde{V}^{\pm} &= -\frac{E_g}{2} - \hbar\omega_l^+(\Lambda_+\Lambda_- + \tfrac{1}{2}) + \frac{P_B^2}{2m_B^+} \pm \tfrac{1}{2}\tilde{g}_l^+\mu_B B \\ \tilde{C}^{\pm} &= +\frac{E_g}{2} + \hbar\omega_l^-(\Lambda_+\Lambda_- + \tfrac{1}{2}) + \frac{P_B^2}{2m_B^-} \pm \tfrac{1}{2}\tilde{g}_l^-\mu_B B. \end{aligned} \tag{27}$$

Here, Λ_+ and Λ_- denote the raising and lowering operators for the transformed wavefunctions

$$\begin{aligned} \Lambda_+|n\rangle &= (n+1)^{1/2}|n+1\rangle \\ \Lambda_-|n\rangle &= n^{1/2}|n-1\rangle \end{aligned} \tag{28}$$

and $P_B = (\hbar/\mathrm{i})\partial/\partial z'$, in which z' is the direction of a magnetic field in the transformed coordinate system. The transformed parameters are

$$\begin{aligned} \tilde{\omega}_c &= 2eBv_B^2/E_g \\ m_B &= E_g v_B^4/2v_l^2 v_t^4 \\ \tilde{\omega}_l^{\pm} &= eB\left(\frac{\lambda_z^2}{m_t^{\pm 2}} + \frac{\lambda_x^2}{m_t^{\pm} m_l^{\pm}}\right)^{1/2} \\ m_B^{\pm} &= \lambda_z^2 m_l^{\pm} + \lambda_x^2 m_t^{\pm} \\ \tilde{g}_l^{\pm} &= (\lambda_z^2 v_t^2 g_l^{\pm} + \lambda_x^2 v_l v_t g_t^{\pm})/v_B^2 \\ \tilde{g}_t^{\pm} &= -\lambda_x\lambda_z(v_t v_l g_l^{\pm} - v_t^2 g_t^{\pm})/v_B^2. \end{aligned} \tag{29}$$

The $g_t^{\pm}$ terms in the matrix (equation (26)) are small and they will be neglected in the following. If, again, one is interested in the case $k_B = 0$, the wavefunction of the form (18) (with transformed coordinates) is a solution of the problem. Its substitution reduces the set of differential equations to a set of linear equations for the coefficients a_i and the energies are given again by equations (19)-(21), in which all parameters are to be substituted by the corresponding parameters with a tilde in equations (29). The latter depend on the direction of magnetic field. The requirement (22) is necessary, to ensure that the raising and lowering operators $\Lambda_\pm$ on the diagonal (cf equations (27)) are the same as the off-diagonal ones in the matrix (26). Since in lead chalcogenides one deals with four ellipsoids along [111] crystal directions, for any direction of magnetic field (with the exception of $\boldsymbol{B} \parallel [001]$) we have at least two non-equivalent energy valleys.

The theory presented above has been successfully used to describe numerous magneto-optical experiments

on non-magnetic lead salts (e.g. Bauer 1980, 1991, McKnight and Drew 1980, Pascher *et al* 1988a).

As mentioned before, the bands in lead chalcogenides deviate slightly from an exact ellipsoidal shape. In the presence of a magnetic field this is manifested by the presence of g_1 terms in equation (26) and the fact that the far-band contributions to the masses do not satisfy exactly the relations of equations (22). If these features are taken into account, the solutions (18) are not valid and one has to look for solutions in terms of sums of harmonic oscillator functions, as first shown by Evtuhov (1962) for the valence bands of Ge. The eigenvalue problem, given by equations (12) and (26), can be then reduced to a diagonalization of a number matrix (this is described in more detail in section 2.2). We have performed such a calculation and it has turned out that, for the realistic values of band parameters of PbTe and PbSe, the deviations from the ellipsoidal shape give negligible contributions to the energies.

2.2. Landau and spin levels in semimagnetic lead chalcogenides

We treat the effect of the paramagnetic ions on orbit and spin properties of mobile carriers in the mean field approximation (cf Galazka and Kossut 1980). In this approach the exchange interaction between the ions and the carriers has the form

$$\hat{H}_{\text{exch}} = J(\boldsymbol{r} - \boldsymbol{R})\boldsymbol{S}\cdot\boldsymbol{\sigma} \tag{30}$$

where $\boldsymbol{\sigma}$ is the carrier spin operator, $\boldsymbol{S}$ is the spin operator of the magnetic ion and J is a coupling constant. We shall assume an external magnetic field to be in the x, z plane. Since the average magnetization of the ions has the same direction as the field; we have

$$\hat{H}_{\text{exch}} = S_0 J(\sin\phi\,\sigma_x + \cos\phi\,\sigma_z) \tag{31}$$

where ϕ is the angle between $\boldsymbol{H}$ and the z axis (parallel to the $\langle 111\rangle$ crystal direction). We have to calculate the Hamiltonian (equation (31)) in the basis of the band-edge functions (equations (8)–(10)). We have

$$\begin{aligned} \langle V^+|J\sigma_z|V^+\rangle &= a_1 - a_2 & \langle C^+|J\sigma_z|C^+\rangle &= b_1 - b_2 \\ \langle V^-|J\sigma_z|V^-\rangle &= a_2 - a_1 & \langle C^-|J\sigma_z|C^-\rangle &= b_2 - b_1 \end{aligned} \tag{32}$$

where

$$\begin{aligned} a_1 &= (1/\Omega_0)\langle R|J|R\rangle\cos^2\theta^+ \\ a_2 &= (1/\Omega_0)\langle S_\pm|J|S_\pm\rangle\sin^2\theta^+ \\ b_1 &= (1/\Omega_0)\langle Z|J|Z\rangle\sin^2\theta^- \\ b_2 &= (1/\Omega_0)\langle X_\pm|J|X_\pm\rangle\cos^2\theta^- \end{aligned} \tag{33}$$

in which Ω_0 is the volume of the unit cell and the integrals are performed over this volume. The off-diagonal matrix elements of the $J\sigma_z$ operator vanish. Similarly, we calculate

$$\begin{aligned} \langle V^+|J\sigma_x|V^-\rangle &= a_1 \\ \langle C^+|J\sigma_x|C^-\rangle &= -b_1. \end{aligned} \tag{34}$$

All the other matrix elements of the operator $J\sigma_x$ vanish. For the PbSe conduction band symmetry (cf equation (10)), one should replace $\sin^2\theta^-\cos^2\theta^-$ in the definition of b_1 (equation (33)) and vice versa in the definition of b_2. Thus the exchange matrix in our basis has the form

$$\begin{bmatrix} A\cos\phi & a_1\sin\phi & 0 & 0 \\ a_1\sin\phi & -A\cos\phi & 0 & 0 \\ 0 & 0 & B\cos\phi & b_1\sin\phi \\ 0 & 0 & -b_1\sin\phi & -B\cos\phi \end{bmatrix} \tag{35}$$

where $A = a_1 - a_2$ and $B = b_1 - b_2$.

The complete Hamiltonian consists now of two parts: the $\boldsymbol{P}\cdot\boldsymbol{\pi}$ part (13) and the exchange part (35).

If the external magnetic field is parallel to the $\langle 111\rangle$ direction, the exchange matrix is diagonal for the band ellipsoid elongated in that direction. In this case the exchange interaction (equation (35)) contributes only additional c-numbers to the diagonal of the $\boldsymbol{P}\cdot\boldsymbol{\pi}$ matrix (equation (13)), so that the solutions (equation (18)) remain valid. This in turn means that the resulting energies are still given by equations (19) and (20), in which $\tilde{a}_n$, $\tilde{b}_n$, $\tilde{c}_n$, $\tilde{d}_n$ of eqution (21) should be replaced by the primed quantities

$$\begin{aligned} \tilde{a}'_n &= \tilde{a}_n + B & \tilde{c}'_n &= \tilde{c}_n - B \\ \tilde{b}'_n &= \tilde{b}_n - A & \tilde{d}'_n &= \tilde{d}_n + A. \end{aligned} \tag{36}$$

If the magnetic field is in the (x, z) plane, one has to apply the transformation (equation (24)) to the sum of the $\boldsymbol{P}\cdot\boldsymbol{\pi}$ part (equation (13)) and the exchange part (equation (35)). Since the transformation is additive, the $\boldsymbol{P}\cdot\boldsymbol{\pi}$ part has the previous form (equation (26)), while the exchange part is obtained as

$$\begin{bmatrix} A\cos\phi\cos\gamma & -A\cos\phi\sin\gamma & 0 & 0 \\ +a_1\sin\phi\sin\gamma & +a_1\sin\phi\cos\gamma & & \\ -A\cos\phi\sin\gamma & -A\cos\phi\cos\gamma & 0 & 0 \\ +a_1\sin\phi\cos\gamma & +a_1\sin\phi\sin\gamma & & \\ 0 & 0 & B\cos\phi\cos\gamma & -B\cos\phi\sin\gamma \\ & & -b_1\sin\phi\sin\gamma & -b_1\sin\phi\cos\gamma \\ 0 & 0 & -B\cos\phi\sin\gamma & -B\cos\phi\cos\gamma \\ & & -b_1\sin\phi\cos\gamma & +b_1\sin\phi\sin\gamma \end{bmatrix} \tag{37}$$

In this general case the non-diagonal exchange terms prevent the solutions of the type of equation (18).

In order to find the eigenvalues we resort to a procedure used for the first time by Evtuhov (1962) to non-spherical valence bands of Ge, and employed since to many other cases (see Pfeffer and Zawadzki 1990). We look for solutions of the problem (equation (12)), in which the Hamiltonian is given by the sum of equation (26) and equation (37), taking the four envelope functions in the form

$$f_l(\boldsymbol{r}') = \exp(\mathrm{i}k_B z') \sum_{m=0}^{\infty} c_m^{(l)} |m\rangle \tag{38}$$

where $c_m^{(l)}$ are coefficients and $|m\rangle$ are the Landau solutions of the problem without exchange terms (cf equation (17)) in the rotated coordinate system.

As before we shall be interested in the case $k_B = 0$ and we put $g_1^+ = 0$. We insert the envelopes (equation (38)) into the complete eigenvalue problem and perform the raising and lowering operations prescribed by the $\boldsymbol{P} \cdot \boldsymbol{\pi}$ matrix (equation (26)). Next, each of the four equations is multiplied on the left by $\langle 0|$ and integrated over the crystal volume. This leaves only the c_m^l coefficients in front of $\langle 0|$ functions and nullifies the rest. Next, one multiplies the equations by $\langle 1|$ and performs the integration. This leaves only the coefficients in front of the $\langle 1|$ function and nullifies the rest. The same procedure is repeated for higher functions $\langle m'|$, transforming the differential problem (equation (4)) into an infinite algebraic set of equations for the coefficients $c_m^{(l)}$ where $l = 1, 2, 3, 4$ and $m = 0, 1, \ldots$.

The condition that the determinant of the set vanishes, furnishes in principle the eigenvalues. It turns out that the infinite set of equations decouples in general into two independent sets. The two matrices have the following forms

where V_n^+, V_n^-, C_n^+, C_n^- are given by $\tilde{d}_n$, $\tilde{b}_n$, $\tilde{a}_n$, $\tilde{c}_n$ of equations (14) and (15) respectively, with the modified parameters of equation (29) and (35). The quantity η is given by $\eta = (E_g \hbar\tilde{\omega}_c)^{1/2}$. All the other terms not indicated in equations (39) and (40) are zero.

The symbols a, b, c and d are given by

$$\begin{aligned} a &= B^*(+A\cos\gamma\cos\phi + a_1 \sin\gamma\sin\phi) \\ b &= B^*(+B\cos\gamma\cos\phi - b_1 \sin\gamma\sin\phi) \\ c &= B^*(-A\sin\gamma\cos\phi + a_1 \cos\gamma\sin\phi) \\ d &= B^*(-B\sin\gamma\cos\phi - b_1 \cos\gamma\sin\phi) \end{aligned} \tag{41}$$

where B^* is the modified Brillouin function according to Gaj *et al* (1979)

$$B^* = \tfrac{1}{2} S_0 x B_S\left(\frac{2S\mu_B|B|}{k_B(T + T_0)}\right) \tag{42}$$

where S is either 5/2 or 7/2 for Mn^{2+} or Eu^{2+} ions, respectively, B_S is the Brillouin function, S_0 and T_0 are parameters determined either from magnetization data (Gorska and Anderson 1988) or from fits to CARS results.

If there are no exchange terms, the above matrices factorize into 2×2 blocks, which give the previously described energies for magnetic field in the (x, z) plane. The exchange terms couple the blocks and, for practical reasons, one has to truncate the infinite matrices in order to calculate the eigenvalues.

This procedure has been applied in all the descriptions of the experimental data, shown below. The exchange terms influence not only the energy eigenvalues of mobile carriers but also their wavefunctions. This results in additional magneto-optical transitions in semimagnetic materials, as compared with those observed in PbTe and PbSe. In particular, the non-diagonal exchange terms, shown in equations (35) or (37), mix the states of the opposite spin. This gives the possibility of a combined

$$\begin{bmatrix}
V_0^- - a - E & c & & & & & & & & & \\
c & V_0^+ + a - E & \eta\sqrt{1} & & & & & & & & \\
 & \eta\sqrt{1} & C_1^- - b - E & 0 & d & & & & & & \\
 & & 0 & V_2^- - a - E & \eta\sqrt{2} & c & & & & & \\
 & & d & \eta\sqrt{2} & C_1^+ + b - E & 0 & & & & & \\
 & & & c & 0 & V_2^+ + a - E & \eta\sqrt{3} & & & & \\
 & & & & & \eta\sqrt{3} & C_3^- - b - E & 0 & d & & \\
 & & & & & & 0 & V_4^- - a - E & \eta\sqrt{4} & c & \\
 & & & & & & d & \eta\sqrt{4} & C_3^+ + b - E & & \\
 & & & & & & & c & & &
\end{bmatrix} \tag{39}$$

$$\begin{bmatrix}
C_0^- - b - E & 0 & d & & & & & & & & \\
0 & V_1^- - a - E & \eta\sqrt{1} & c & & & & & & & \\
d & \eta\sqrt{1} & C_0^+ - b - E & 0 & & & & & & & \\
 & c & 0 & V_1^+ + a - E & \eta\sqrt{2} & & & & & & \\
 & & & \eta\sqrt{2} & C_2^- - b - E & 0 & d & & & & \\
 & & & & 0 & V_3^- - a - E & \eta\sqrt{3} & c & & & \\
 & & & & d & \eta\sqrt{3} & C_2^+ + b - E & 0 & & & \\
 & & & & & c & 0 & V_3^+ + a - E & \eta\sqrt{4} & & \\
 & & & & & & & \eta\sqrt{4} & C_4^- - b - E & &
\end{bmatrix} \tag{40}$$

cyclotron-spin resonance and spin resonances for the light polarized parallel to magnetic field (in the Voigt configuration). Such resonances have been indeed observed, as shown below. We do not quote the calculations for the lack of space. It should be noted, that the numerical results for the Landau levels calculated previously (Pascher *et al* 1989, Röthlein *et al* 1990) are identical to those obtained using equations (39) and (40).

Figures 3 and 4 show Landau levels in the conduction and valence bands of $Pb_{1-x}Mn_xTe$ and $Pb_{1-x}Eu_xSe$, respectively, as calculated with the parameters listed below. The influence of the exchange interactions is much stronger in the valence band than in the conduction band and it has different sign in the Eu system as compared with the Mn compound.

3. Experiment

As shown in section 2, the primary effect of exchange interaction between the paramagnetic ions and the mobile carriers is to modify the spin splitting of Landau levels. The size and sign of the spin splitting of the Landau levels depend on composition, temperature, magnitude and orientation of applied magnetic field.

In order to get quantitative information on the exchange interactions one has to measure experimentally spin-flip resonances, combined resonances or interband magneto-optical transitions involving spin-flips. In the IV–VI compounds, electric dipole induced spin-flip resonances can be observed as rather weak transitions (as compared with the cyclotron resonance transitions) in far-infrared magnetotransmission or reflectivity. Far-infrared (FIR) lasers or Fourier transform spectroscopy are used as experimental tools. Because of the narrow energy gap of the IV–VI compounds, interband spectroscopy also has to be performed in the infrared.

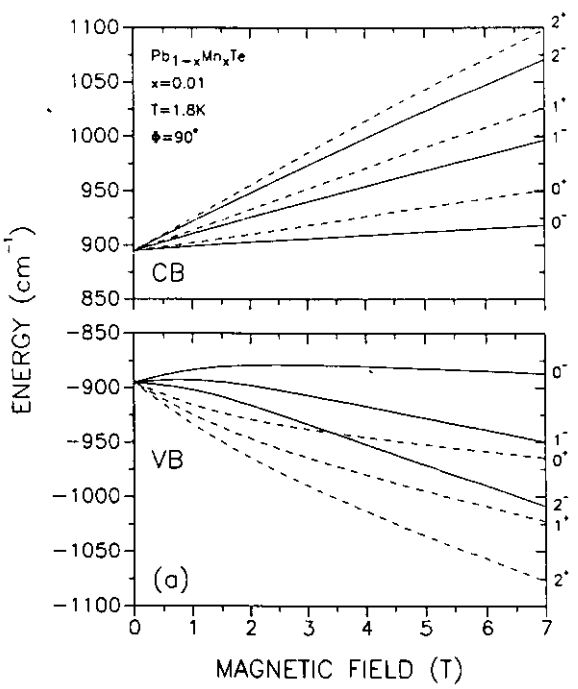

Figure 3. Calculated Landau levels in $Pb_{1-x}Mn_xTe$ versus magnetic field. The effect of exchange interaction between Mn ions and mobile carriers is considerably larger in the valence band.

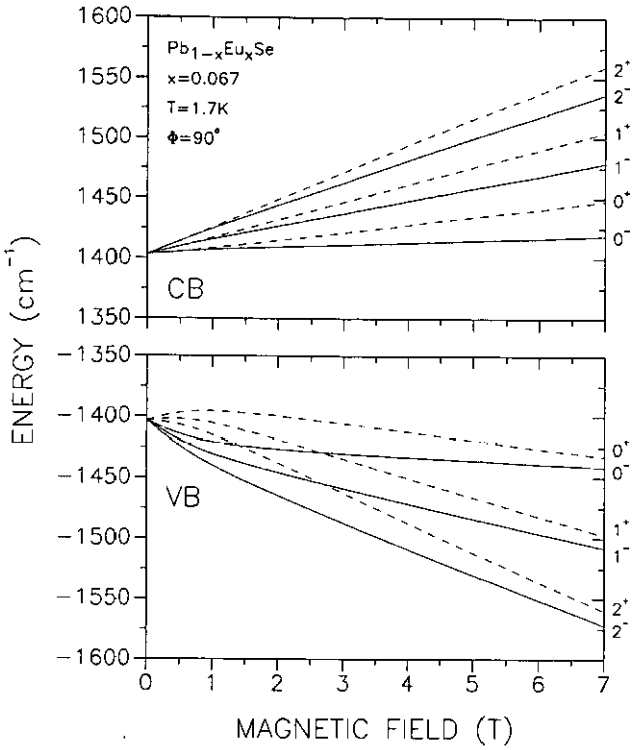

Figure 4. Calculated Landau levels in $Pb_{1-x}Eu_xSe$ versus magnetic field. The signs of exchange integrals are opposite to those in $Pb_{1-x}Mn_xTe$ which is reflected in the behaviour of the valence levels.

Interband magneto-optical transitions observed both in Faraday ($\boldsymbol{k} \parallel \boldsymbol{B}$) and Voigt geometry ($\boldsymbol{k} \perp \boldsymbol{B}$) provide information on the energy gap, selection rules, g-factors and effective masses. High-mobility samples of semimagnetic IV–VI compounds are available as epitaxial films and not as bulk samples. Depending on film orientation only certain magnetic field directions are possible for a given sample: e.g. for samples grown along the [111] direction in the Faraday geometry $\boldsymbol{B}$ is always parallel to the [111] direction whereas for Voigt geometry only orientations of $\boldsymbol{B}$ within the plane of the film are accessible (figure 5). Suitable directions are either $\boldsymbol{B} \parallel [1\bar{1}0]$ or $\boldsymbol{B} \parallel [\bar{1}\bar{1}2]$ for $\boldsymbol{B} \parallel \boldsymbol{E}$ or for $\boldsymbol{B} \perp \boldsymbol{E}$, respectively. Least-squares fits to those data provide energy gaps, matrix elements and anisotropy factors, as presented in tables 1 and 2, respectively. The far-band contributions are assumed to be identical to those found in the non-magnetic host materials, an assumption which is justified by the small content of magnetic ions.

Transmission magnetospectroscopy yields enough information, and no need exists for modulation techniques if one uses epitaxial films a few micrometres thick. Because of the small energy gap, the Landau level structure of the conduction and valence bands has to be probed by mid-infrared techniques. Using various laser lines for magnetospectroscopy, i.e. keeping the frequency of the laser constant and sweeping the magnetic field, the

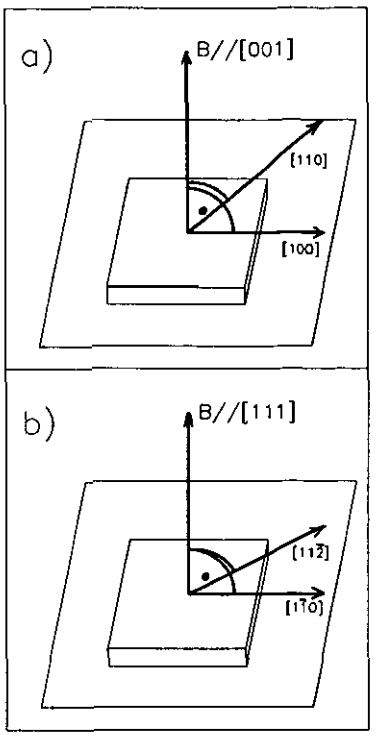

Figure 5. Magnetic field orientations for epitaxial samples. (*a*) Growth axis [001]—Faraday configuration: $\boldsymbol{B} \| [001]$, Voigt configuration: $\boldsymbol{B} \| [110]$ or [100]. (*b*) Growth axis [111]—Faraday configuration: $\boldsymbol{B} \| [111]$, Voigt configuration: $\boldsymbol{B} \| [1\bar{1}0]$ or $[11\bar{2}]$.

resulting spectra determine the Landau level energies and the influence of the magnetization of the magnetic ions on these energies.

The allowed interband transitions for the Faraday geometry are given by the following selection rules: $\Delta n = 0$, $\Delta s = \pm 1$, (σ^+, σ^-). For the Voigt geometry $(\boldsymbol{E} \| \boldsymbol{B} \perp \boldsymbol{k})$ these rules are $\Delta n = 0$, $\Delta s = 0$. Thus from a proper combination of measurements in Faraday and Voigt geometry for more than one orientation of the applied magnetic field, the g-factors of electrons and holes as well as their anisotropy can be deduced from the experimental data. A direct determination of the electron and hole g-factors, their magnetic field and temperature dependence is possible only with the use of spin-flip transitions.

In the epitaxial films, this is conveniently done by applying the magnetic field parallel to the $[1\bar{1}0]$ direction. Then only the two valleys which have their main axes oriented by 35.26° with respect to $\boldsymbol{B}$ contribute to the cyclotron resonance. If the electric field $\boldsymbol{E}$ of the IR radiation is oriented parallel to $\boldsymbol{B}$, it makes the same angle of 35.26° with the main ellipsoid axes as B. For the two other valleys, ϕ is 90° and hence the oscillating E-field cannot induce a cyclotron motion. Spin-flip transitions are easily observed in this $\boldsymbol{E} \| \boldsymbol{B}$ geometry, in a magnetic field sweep, at the fixed FIR laser wavelength the spin-flip resonance (ω_{SF}) appears apart from the cyclotron resonance (ω_c).

A difficulty in the measurements of SF resonances in the FIR is caused by the high carrier concentration in the IV–VI compounds. Instead of a simple resonance, a resonance associated with a dielectric anomaly occurs as long as ω_{SF} is smaller than $\omega_{LO}^+ = \sqrt{\omega_{LO}^2 + \omega_p^2}$ where ω_{LO}^+ denotes the coupled LO phonon plasma frequency, and ω_p the plasma frequency (Bauer 1980, 1991).

Spin-flip transitions can also be measured directly using nonlinear Raman light scattering techniques. De Silets and Patel (1973), Brueck and Mooradian (1973) and Pascher (1984, 1990) have shown that nonlinear four-wave mixing techniques are powerful for the observation of Raman-allowed spin-flip resonances. Since narrow-gap semiconductors like the IV–VI compounds are only transparent for mid-infrared light (3–11 μm), special techniques have to be developed in order to exploit all the advantages. The most important Raman-like resonance of the nonlinear susceptibiltiy $\chi^{(3)}$ is caused by spin-flip transitions. The technique to observe $\chi^{(3)}$ (B) uses a superposition of two laser beams at frequencies ω_L and ω_S with polarizations perpendicular and parallel to B, respectively. The anti-Stokes intensity at $\omega_{AS} = 2\omega_L - \omega_S$ is monitored as a function of applied magnetic field. Whenever the frequency difference corresponds to the spin-flip energy

$$\hbar(\omega_L - \omega_S) = g^* \mu_B B \tag{43}$$

Table 1. Band parameters of PbTe and of $Pb_{1-x}Mn_xTe$ (in the notation of Adler *et al* (1973)).

Parameter	Sample			
	PbTe $x = 0$	$Pb_{1-x}Mn_xTe$ $x = 0.006$	$Pb_{1-x}Mn_xTe$ $x = 0.01$	$Pb_{1-x}Mn_xTe$ $x = 0.012$
E_g (meV)	189.7 ± 0.2	209.8	221.9	225.7
$2P_\perp^2/m_0$ (eV)	6.02 ± 0.05	5.77	5.51	—
$P_\perp/P_\parallel$	3.42 ± 0.05	3.52	3.74	—
m_t^-/m_0	0.060 ± 0.002	0.060	0.060	0.060
m_l^-/m_0	0.505 ± 0.01	0.505	0.505	0.505
m_t^+/m_0	+0.102 ± 0.002	+0.102	+0.102	+0.102
m_l^+/m_0	+0.920 ± 0.02	+0.920	+0.920	+0.920
g_t^-	−1.39 ± 0.02	−1.39	−1.39	−1.39
g_l^-	+1.72 ± 0.02	1.72	1.72	1.72
g_t^+	4.39 ± 0.02	4.39	4.39	4.39
g_l^+	−2.61 ± 0.01	−2.61	−2.61	−2.61

Table 2. Band parameters of PbSe and of $Pb_{1-x}Eu_xSe$.

Parameter	Sample			
	PbSe $x = 0$	$Pb_{1-x}Eu_xSe$ $x = 0.012$	$Pb_{1-x}Eu_xSe$ $x = 0.0142$	$Pb_{1-x}Eu_xSe$ $x = 0.024$
E_g (meV)	146.3 ± 0.3	181.1	189.1	219.0
$2P_\perp^2/m_0$ (eV)	3.6 ± 0.1	3.6	3.6	3.6
$P_\perp/P_\parallel$	1.35 ± 0.02	1.40	1.40	1.40
m_t^-/m_0	0.27 ± 0.05	0.27	0.27	0.27
m_l^-/m_0	0.95 ± 0.2	0.95	0.95	0.95
m_t^+/m_0	+0.29 ± 0.05	+0.29	+0.29	+0.29
m_l^+/m_0	+0.37 ± 0.1	+0.37	+0.37	+0.37
g_t^-	−4.0 ± 1	−4.0	−4.0	−4.0
g_l^-	−8.1 ± 1	−8.1	−8.1	−8.1
g_t^+	5.4 ± 1	5.4	5.4	5.4
g_l^+	7.3 ± 1	7.3	7.3	7.3

the anti-Stokes intensity is resonantly enhanced (coherent anti-Stokes Raman scattering: CARS). In this type of spectroscopy one keeps the laser frequencies ω_L, ω_S fixed and tunes the magnetic field into resonance. The intensity resonances yield precise data on effective g-factors which are of special importance in semimagnetic materials. Nonlinear mixing experiments have been performed so far on $Pb_{1-x}Mn_xTe$ and $Pb_{1-x}Eu_xSe$. Two Q-switched CO_2 laser beams with powers from 100 W to about 2 kW and pulse lengths of about 100 ns were used, short enough to avoid lattice heating.

The anti-Stokes intensity I_{AS} is proportional to L^2, L being the film thickness. In general it is preferable to have one of the two laser lines close to the energy gap ($\hbar\omega_L \approx E_g$), in order to take advantage of the bandgap resonance. It should be noted that for CO_2 laser radiation two-photon absorption is possible in both PbMnTe and PbEuSe (for not too high Mn or Eu contents). Therefore, a considerable number of minority carriers are produced due to the intense pulsed excitation. In this way one can observe simultaneously the electron and hole resonances in both n- and p-type samples.

Four-wave mixing Raman spectroscopy has proved to be a useful tool for the observation of intraband transitions in the narrow-gap diluted magnetic semiconductors. The anisotropy of the g-factors, their magnetic field, temperature and composition dependence can be obtained by this method with higher precision than that obtainable with electric dipole induced spin-flip resonances. This technique can be used to determine spin-flip transitions at fields as low as 0.05 T. It turns out that measurements in the low-magnetic-field region are quite important for the proper description of the exchange-induced effects.

3.1. Magnetization

We present a short overview of the magnetic properties of $A^{IV}_{1-x}Mn_xB^{VI}$ and $A^{IV}_{1-x}Eu_xB^{VI}$ alloys, in as much detail as needed for the interpretation of magneto-optical experiments through the mechanism of the sp-d(f) exchange. The lead compounds are paramagnetic and a weak antiferromagnetic interaction is observed from susceptibility and magnetization measurements. Gorska and Anderson (1988) have postulated that a superexchange interaction via the group VI anions is responsible for the antiferromagnetic interaction between the Mn^{2+}—or Eu^{2+}—ions. As found in semimagnetic II-VI compounds, magnetization experiments can be modelled by a modified Brillouin function (see also equation (42))

$$M = x_{\text{eff}} N_0 g_{\text{Mn(Eu)}} \mu_B S B_S[g_{\text{Mn(Eu)}} \mu_B S B/k_B(T + T_0)] \quad (44)$$

where x_{eff} is the effective Mn(Eu) content, N_0 the number of cations per unit volume μ_B is the Bohr magneton, $S = 5/2(Mn^{2+})$ or $7/2$ (Eu^{2+}), B_S is the Brillouin function T is the lattice temperature and T_0 is an effective temperature. In figure 6 results on epitaxial films of $Pb_{1-x}Mn_xTe$ are shown and in figure 7 results on bulk $Pb_{1-x}Mn_xTe$, and $Pb_{1-x}Mn_xSe$ are compared with calculations (Pascher *et al* 1989, Anderson *et al* 1990).

So far, a step-like behaviour of the magnetization as a function of magnetic field has not been observed. Since in the IV-VI compounds the exchange integrals J for

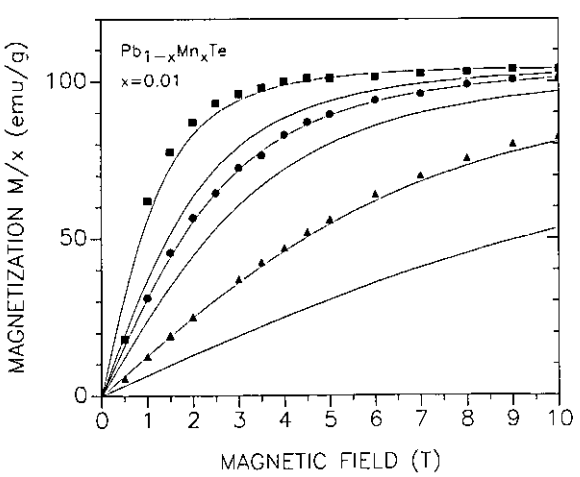

Figure 6. Magnetization of epitaxial $Pb_{1-x}Mn_xTe$ versus magnetic field with T as parameter. Experimental data ■ ($T = 2$ K), ● ($T = 4.2$ K), ▲ ($T = 15$ K). Full curves: calculations based on a modified Brillouin function for $T = 1.8$ K, 3.5 K, 4.4 K, 6.1 K, 12 K and 22 K using the parameters of Gorska and Anderson (1988).

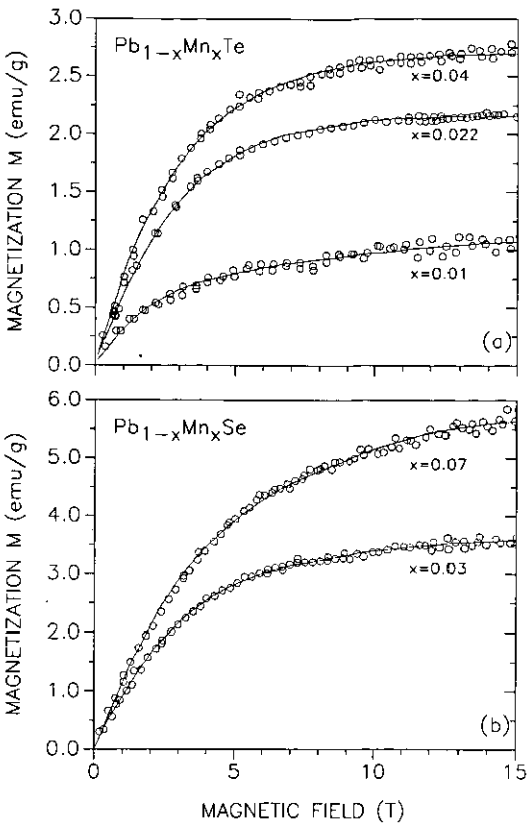

Figure 7. Magnetization of bulk $Pb_{1-x}Mn_xTe$ and $Pb_{1-x}Mn_xSe$ versus magnetic field for $T = 4.2$ K (after Anderson *et al* 1990).

nearest-neighbour Mn^{2+}–Mn^{2+} or Eu^{2+}–Eu^{2+} interaction are smaller than those in the II-VIs, most probably the temperature range investigated (> 2K) was still too high for the observation of magnetization steps. These steps are a direct consequence of the existence of antiferromagnetically coupled Mn^{2+} or Eu^{2+} nearest-neighbour pairs.

Another group of semimagnetic IV-VI materials with high Sn or Ge contents exhibits a ferromagnetic phase which is caused by the indirect exchange interaction via free carriers (holes) (Ruderman-Kittel-Kosiya-Yosida (RKKY)) interaction and which has been extensively studied in $Pb_{1-x-y}Sn_xMn_yTe$ with hole concentration $p \approx 10^{20}$ cm^{-3} (Story *et al* 1986, 1990, de Jonge *et al* 1991, Galazka *et al* 1991). However, these materials have comparatively low mobilities (≈ 200 cm^2 V^{-1} s^{-1}) and thus they are not particularly suitable for magneto-optical investigations.

3.2. Interband magneto-optics

In figure 8 we present magnetotransmission spectra of PbMnSe, PbMnTe and PbEuSe. The experiments were performed in Faraday configuration using σ^+ and σ^- circularly polarized radiation. There exists a remarkable difference between the Mn and Eu compounds: in the former the σ^+ resonances occur for a given photon energy at higher magnetic fields than the σ^- resonances. For $Pb_{1-x}Eu_xSe$ just the opposite is observed. From the

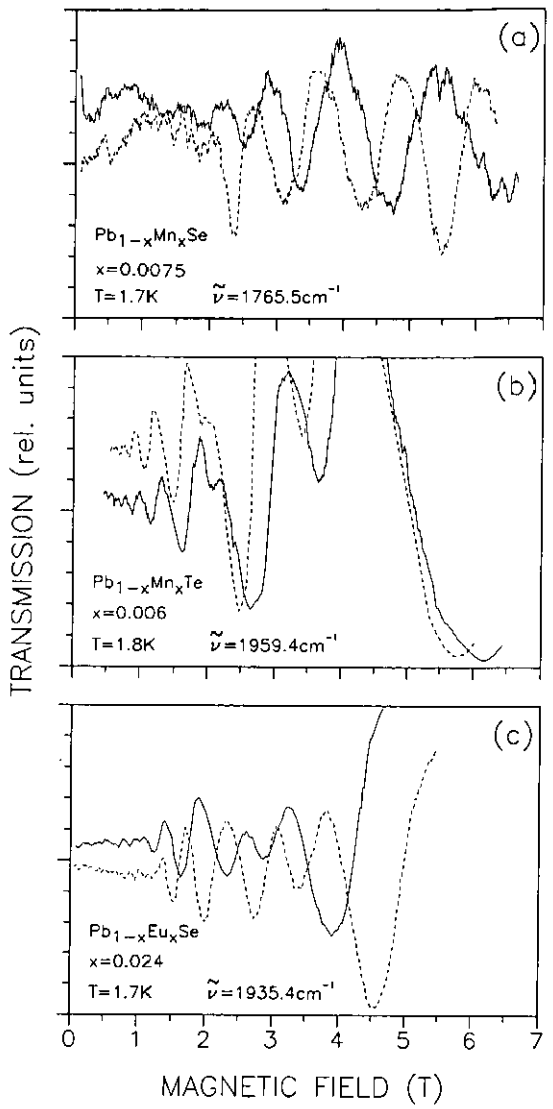

Figure 8. Interband magnetotransmission for Faraday geometry ($\boldsymbol{B} \| \boldsymbol{k}[111]$) for (*a*) $Pb_{1-x}Mn_xSe$, (*b*) $Pb_{1-x}Mn_xTe$ and (*c*) $Pb_{1-x}Eu_xSe$. Full curves for σ^+ and broken curves for σ^- circularly polarized radiation. For the Mn compounds transmission minima occur at lower fields for σ^- radiation in comparison with those for σ^+ radiation; the opposite is observed for $Pb_{1-x}Eu_xSe$.

selection rules $|n, + \rangle \rightarrow |n, - \rangle$ or $|n, - \rangle \rightarrow |n, + \rangle$ and from the comparison with the spectra of the binary compounds PbTe and PbSe one can conclude that the overall effect on the g-factors in the Mn- and Eu-based systems will be of opposite sign.

A detailed analysis of the data, based on the above presented theory, as shown in figures 9 and 10, indicates that the dominant exchange integrals related to the Mn ions have the opposite signs to those of the Eu ions. In addition it turns out that the exchange interaction of the magnetic ions with holes is much larger than that with electrons.

In Voigt geometry, the selection rules for $\boldsymbol{E} \| \boldsymbol{B} \perp \boldsymbol{k}$ are $\Delta n = 0$, $\Delta s = 0$. However, in the semimagnetic case for $Pb_{1-x}Mn_xTe$, $\Delta n = 0$ also, but $\Delta s = \pm 1$ (broken curves in figure 9) become observable, which indicates that the presence of magnetic ions relaxes the selection rules.

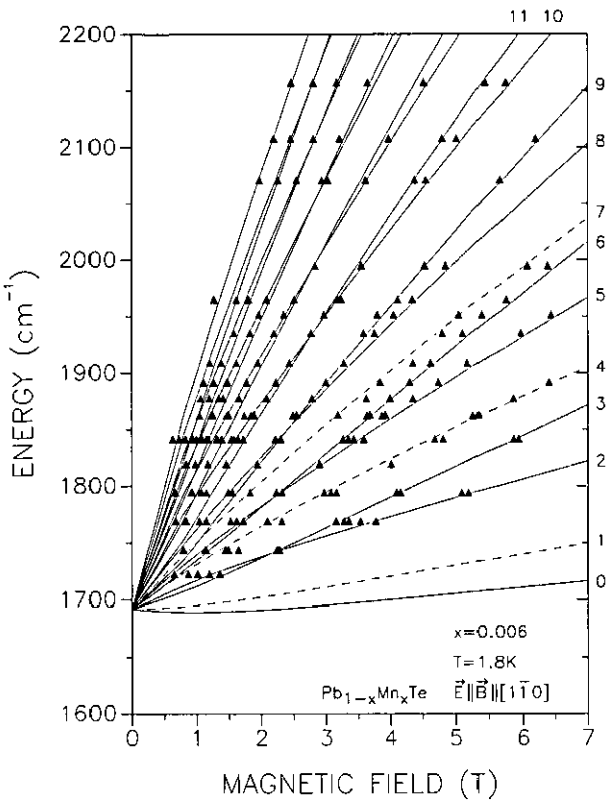

Figure 9. Fan chart for interband magneto-optical transition in the Voigt geometry for $Pb_{1-x}Mn_xTe$, $\boldsymbol{E}\|\boldsymbol{B}\|[1\bar{1}0]$. Experimental data, ▲, in $\boldsymbol{E}\|\boldsymbol{B}$ polarization. Full curves: calculated values for $\phi = 90°$; broken curves: $\phi = 35.26°$. 0: $0^- \rightarrow 0^-$ ($\phi = 90°$); 1: $0^- \rightarrow 0^-$ ($\phi = 35.26°$); 2: $0^+ \rightarrow 0^+$ ($\phi = 90°$); 3: $1^- \rightarrow 1^-$ ($\phi = 90°$); 4: $0^+ \rightarrow 0^-$ ($\phi = 35.26°$); 5: $1^+ \rightarrow 1^+$ ($\phi = 90°$); 6: $2^- \rightarrow 2^-$ ($\phi = 90°$); 7: $0^+ \rightarrow 0^+$ ($\phi = 35.26°$); 8: $2^+ \rightarrow 2^+$ ($\phi = 90°$); 9: $3^- \rightarrow 3^-$ ($\phi = 90°$); 10: $3^+ \rightarrow 3^+$ ($\phi = 90°$); 11: $4^- \rightarrow 4^-$ ($\phi = 90°$). (After Pascher *et al* 1989.)

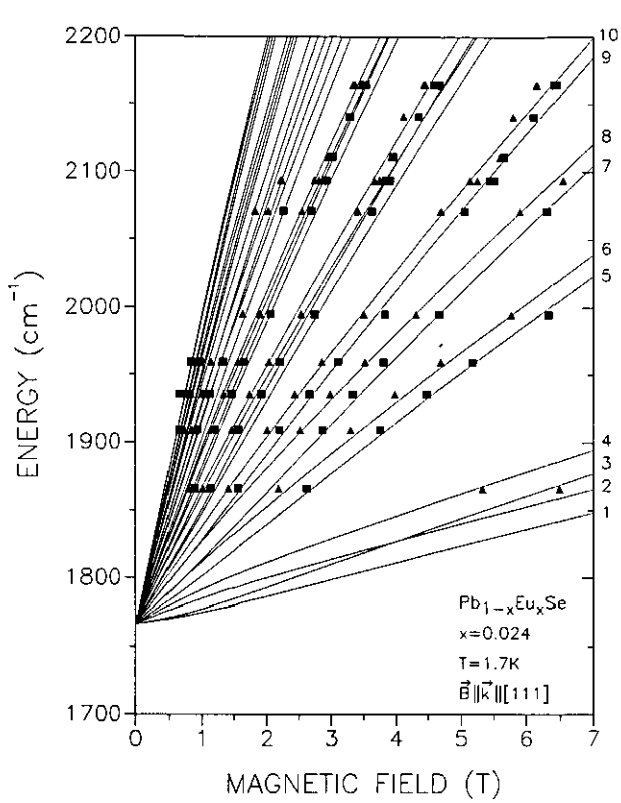

Figure 10. The same as in figure 9 but for $Pb_{1-x}Eu_xSe$ in the Faraday geometry ($\boldsymbol{B}\|\boldsymbol{k}[111]$). Experimental data for σ^- (■) and σ^+ (▲) transitions. Full curves: calculated data; identification: 1: $0^+ \rightarrow 0^-$ ($\phi = 70.53°$), 2: $0^- \rightarrow 0^+$ ($\phi = 70.53°$), 3: $0^+ \rightarrow 0^-$ ($\phi = 0°$), 4: $0^- \rightarrow 0^+$ ($\phi = 0°$), 5: $1^+ \rightarrow 1^-$ ($\phi = 70.53°$), 6: $1^- \rightarrow 1^+$ ($\phi = 70.53°$), 7: $1^+ \rightarrow 1^-$ ($\phi = 0°$), 8: $1^- \rightarrow 1^+$ ($\phi = 0°$), 9: $2^+ \rightarrow 2^-$ ($\phi = 70.53°$), 10: $2^- \rightarrow 2^+$ ($\phi = 70.53°$). (After Röthlein *et al* 1990.)

Least-square fits to these data provide energy gaps, interband matrix elements and anisotropy factors as presented in tables 1–3, respectively. The far-band contributions are assumed to be identical to those found in the diamagnetic host materials, an assumption which is justified by the small content of magnetic ions.

To determine the g-factor of holes and electrons for [001]-oriented $Pb_{1-x-y}Mn_xSn_ySe$ films ($B\|[001]$), Zasavitskii and co-workers (Zasavitskii and Sazonov 1988, Zasavitskii *et al* 1988) used interband magneto-optical transitions. As a function of Mn concentration the hole g-factor increases, while the electron g-factor decreases. The interband experiments were also used by Kowalczyk (1991) to study $Pb_{1-x}Mn_xSe$. The influence of external fields on stimulated emission from p–n junctions was studied. The results of both investigations are qualitatively similar (figures 11(*a*) and 11(*b*)).

3.3. Intraband magneto-optics

Magneto-optical intraband transitions in Faraday and Voigt geometry as well as in stripline geometry have been investigated so far using PbMnTe epitaxial films. With $\boldsymbol{B}\|[111]$ two resonant frequencies associated with the cyclotron resonances of the (111) and the three oblique {111} valleys have been observed (Niedwodniczanska-Zawadzka *et al* 1983, von Ortenberg *et al* 1985, Gorska *et al* 1984).

In n-type samples with high mobilities both $|n, -\rangle \rightarrow |n+1, -\rangle$ as well as $|n, +\rangle \rightarrow |n+1, +\rangle$ transitions can be observed from which the effective masses are deduced. With respect to the semimagnetic properties, more interesting information is extracted from experiments in Voigt geometry, which involves spin-flip transitions. For the PbTe band structure just the 35° valleys should yield a cyclotron resonance absorption whereas the 90° valleys do not yield any absorption at all (von Ortenberg 1980, Bauer 1991). This is indeed observed. In the PbMnTe samples, however, an additional line appears which is identified from Landau level calculations to be associated with a spin-flip transition in the 35° valleys (figure 12). The corresponding transition energies are shown in figure 13 for $x = 0.01$. Whereas in PbTe the spin-flip resonance is only weakly allowed because of non-parabolicity effects (Schaber and Doezema 1979) the presence of Mn ions appreciably increases the oscillator strength. Also the holes in PbMnTe samples exhibit spin-flip transitions which are much stronger than the corresponding ones in PbTe. Since the transition energies of the spin-flip process reflect the strong dependence of the

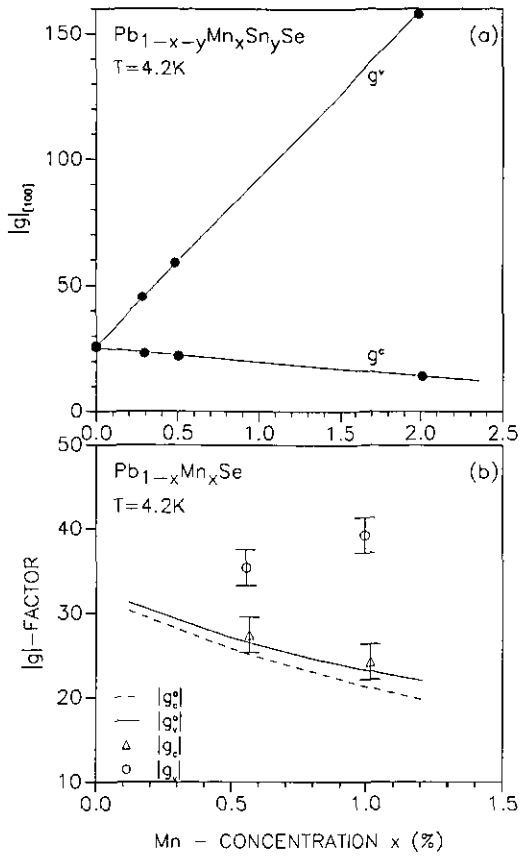

Figure 11. Valence and conduction band *g*-factors as determined from interband magnetoluminescence experiments on (*a*) $Pb_{1-x-y}Mn_xSn_ySe$ (Zasavitskii *et al* 1988) for $\boldsymbol{B} \parallel [001]$ and (*b*) for $Pb_{1-x}Mn_xSe$ (Kowalczyk 1991). With increasing Mn content the valence band *g*-factors increase whereas the conduction band *g*-factors decrease. Broken and full curves represent change of *g*-factors with Mn composition due to increase of the energy gap but without the exchange correction.

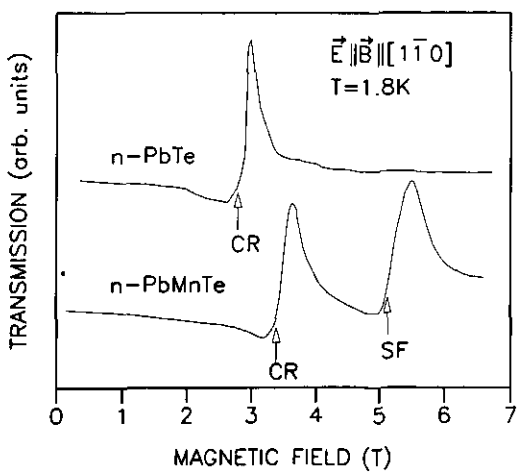

Figure 12. Far-infrared magnetotransmission in the Voigt geometry for PbTe and $Pb_{1-x}Mn_xTe$. Apart from the cyclotron resonance of the $\phi = 35.26°$ valleys a spin-flip resonance appears for $Pb_{1-x}Mn_xTe$. In PbTe just the oblique valley resonance ($\phi = 35.26°$) is observed, whereas in $Pb_{1-x}Mn_xTe$ an additional resonance identified as a spin-flip resonance occurs. (From Bauer 1991.)

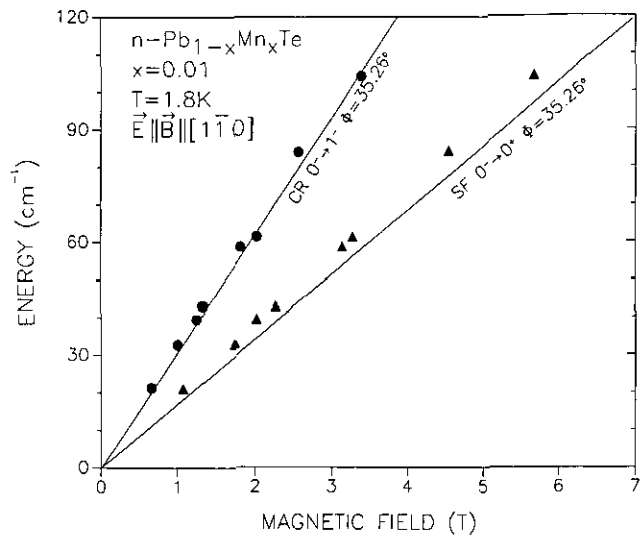

Figure 13. Fan chart of cyclotron resonance (●) and spin-flip (▲) energies of electrons in $Pb_{1-x}Mn_xTe$ versus magnetic field. Full lines: calculated transition energies. (From Pascher *et al* 1989.)

exchange-induced effects for holes, the corresponding transition energies, as shown in figure 14, depend in a strongly nonlinear fashion on the applied magnetic field. The experimentally observed dependence is well accounted for by the calculated transition energies.

The use of stripline transmission spectroscopy in the FIR enhances its sensitivity and allows one to detect weak transitions. In figure 15 we show such data for the Voigt geometry on n-PbMnTe. In addition to the resonances already observed in straightforward transmission, new resonances appear as shown in figure 16. The fan chart exhibits not only the cyclotron and spin-flip resonances but also three other transitions designated by $|_1$, $|_2$, $|_3$. Such additional lines were observed for Mn contents from 1% to 1.9% in n-type material. The origin of these transitions is at present not understood.

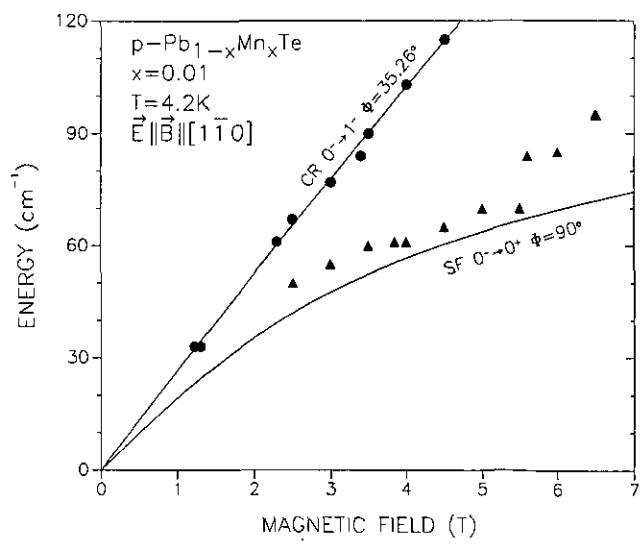

Figure 14. The same as in figure 11, but for holes. The spin-flip resonances show a strong nonlinear dependence on *B*. (From Pascher *et al* 1989.)

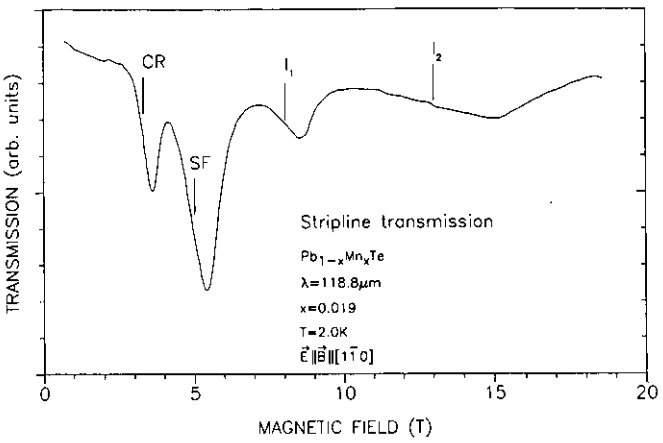

Figure 15. Magnetotransmission of $Pb_{1-x}Mn_xTe$ versus B in stripline geometry. Besides the cyclotron and spin-flip resonances further resonances marked l_1, l_2 are observed. (From von Ortenberg *et al* 1985.)

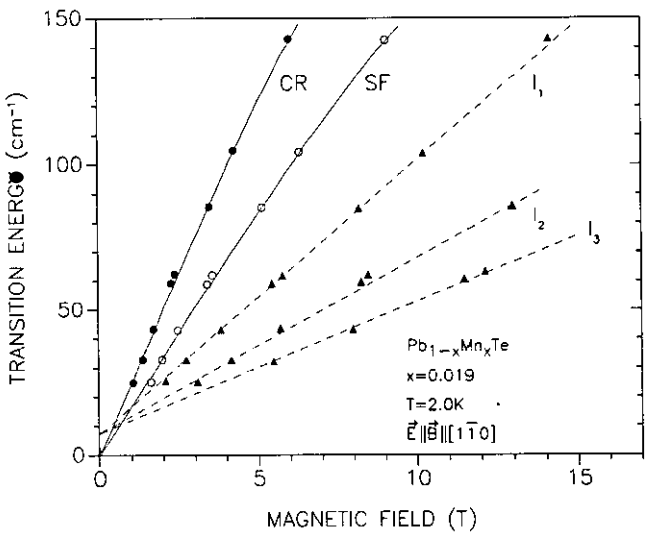

Figure 16. Fan chart of far-infrared magnetotransmission of $Pb_{1-x}Mn_xTe$ versus magnetic field. The origin of the three transitions (l_1, l_2, l_3) marked by triangles and broken curves is at present not understood.

3.4. Four-wave mixing

In figure 17(*a*) we show the CARS intensity versus applied field for a p-type PbMnTe sample. Figure 17(*b*) exhibits the temperature dependence of the resonant positions. The resonances labelled 'a' and 'b' correspond to electrons in valleys oriented 35° and 90° with respect to the applied B-field. The curves 'c' and 'd' correspond to holes for the two types of valley. Whereas the electron resonances shift with increasing temperature to lower fields, hole resonances shift to higher fields. The absolute magnitude of this shift is much higher for holes than for electrons, demonstrating directly that the exchange interaction has a much stronger effect on the holes.

The effective g-factors are deduced using equation (43). The results are summarized in figure 18 for a wide range of fields at a fixed temperature $T = 1.8$ K. It can be seen that in $Pb_{1-x}Mn_xTe$ the exchange interaction leads to a strong enhancement of the hole g-factors and a

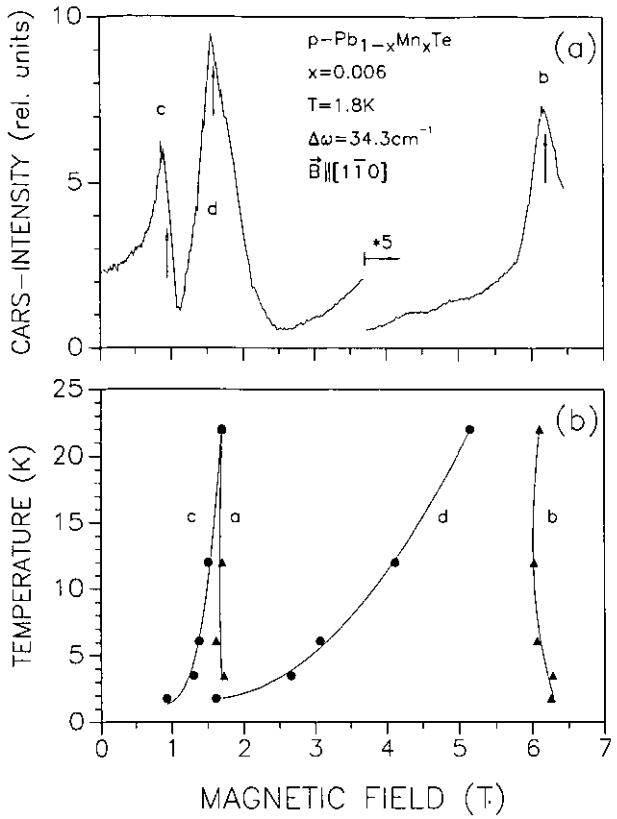

Figure 17. (*a*) CARS intensity for $Pb_{1-x}Mn_xTe$ versus B for fixed energy difference $\omega_L - \omega_S = 34.3\,cm^{-1}$. The resonance marked 'b' is due to electrons in the two valleys with $\phi = 90°$, 'c' and 'd' are due to holes with $\phi = 35.26°$ and 90° valleys, respectively. (*b*) Shift of resonant magnetic fields with increasing temperature for electrons ('a, b': $\phi = 35.36°$ and 90°, respectively) and holes ('c, d': $\phi = 35.26°$ and 90°, respectively). (From Pascher *et al* 1989.)

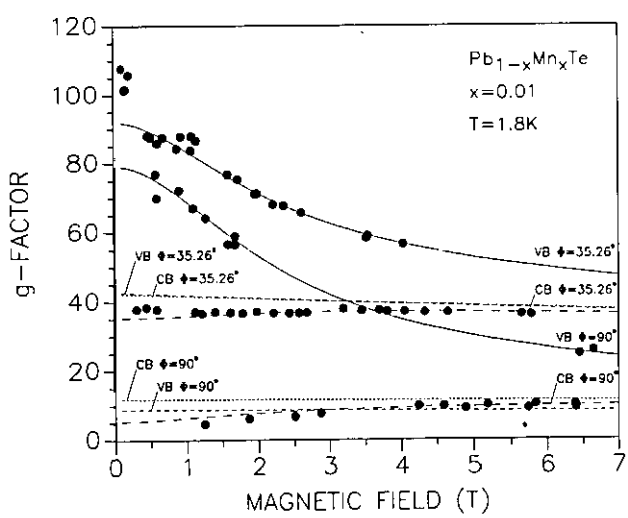

Figure 18. Magnetic field dependence of g-factors in $Pb_{1-x}Mn_xTe$. Experimental data (●) for electrons ($\phi = 35.26°$, $\phi = 90°$, conduction band, CB) and for holes (valence band, VB). Full curves show the calculated values for holes and broken curves those for electrons. Dotted curves: calculated magnetic field dependences of g-factors (electrons and holes) due to band non-parabolicity, neglecting exchange effects. Experimental data show that exchange corrections increase hole g-factors for $\phi = 35.26°$ and $\phi = 90°$ valleys and decrease those for electrons. (From Pascher 1990.)

decrease of the electron g-factors. For sufficiently high magnetic fields (i.e. saturated magnetization) the measured g-factors approach values determined by the band structure without exchange interaction either from above (holes) or from below (electrons)., The calculated dependences of $g^*(B)$ agree well with the observed ones, with the exception of few points at the lowest fields. This should not be surprising, since at low magnetic fields and low temperatures the mean-field approximation, used in the theoretical description, breaks down. On the other hand, one cannot exclude larger experimental errors at these low fields. The dependence of the g-factor on temperature (at a fixed low magnetic field of $B = 0.05$ T) reflects the temperature dependence of the magnetization. Again, at low temperature the exchange effects are strong (figure 19) and lead to a substantial increase of the hole g-factors and to a smaller decrease of the electron g-factors. With increasing temperature, the exchange-induced corrections diminish. At temperatures greater than 20 K these corrections are barely observable in samples with low Mn content.

The CARS experiments were made on three samples with Mn contents 0.6, 0.8 and 1 %. Figure 20 shows the measurements of the CARS intensity resonances, keeping $\hbar(\omega_L - \omega_S)$ constant and sweeping the magnetic field. The data of figure 20 have been used to determine the g-factor values. The calculations by the theory outlined above represent very well the observed data. From these data not only the four exchange parameters (see table 3) but also S_0 and T_0 are obtained. The latter agree quite well with the parameters given by Gorska and Anderson (1988).

$Pb_{1-x}Eu_xSe$ has been studied by the CARS method for Eu concentrations up to about 7 %. Figure 21 shows the CARS intensity versus B for fixed frequency difference $\Delta\omega = 32\ \mathrm{cm}^{-1}$ which corresponds to the spin-flip transition energy. For $\boldsymbol{B} \| [1\bar{1}0]$, electron and hole resonances marked 'c', 'd' and 'a', 'b' respectively, are observed for the 35° ('c','a') and 90° valleys ('d','b'). With increasing temperature, the resonance positions shift appreciably as

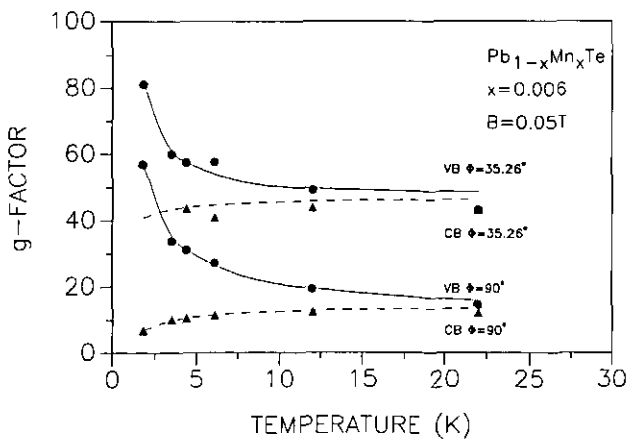

Figure 19. Temperature dependence of electron (▲) and hole (●) g-factors for the $\phi = 35.25°$ and 90° valleys for $Pb_{1-x}Mn_xTe$. Broken curves for electrons (CB) and full lines for holes (VB) are calculated.

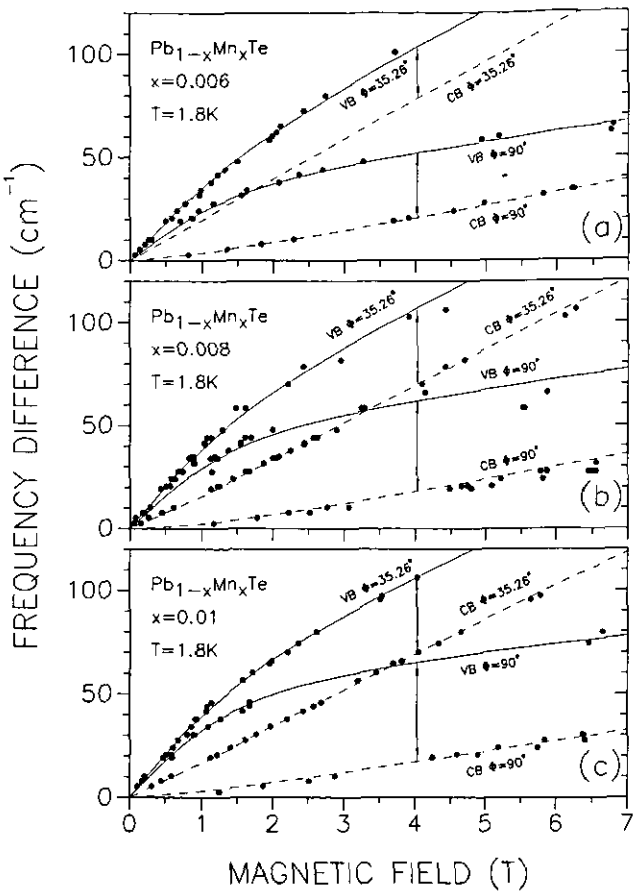

Figure 20. CARS measurements on $Pb_{1-x}Mn_xTe$ for three compositions $x = 0.006$, $x = 0.008$ and $x = 0.01$ at $T =$ 1.8 K. Experimental data (●) are spin-flip transition energies ($0^- \rightarrow 0^+$). Full curves: calculated values for spin-flip transitions of holes (VB) in $\phi = 35.26°$ and 90° valleys. Broken curves: the same for electrons.

shown in figure 21(b). However, as seen by comparison with figure 17, the resonance positions in $Pb_{1-x}Mn_xTe$ and $Pb_{1-x}Eu_xSe$ show different T_{res} versus B_{res} dependences.

In figure 22 the frequency difference $\hbar(\omega_L - \omega_S)$ versus B (i.e. the spin-flip transition energy) is shown for five samples with Eu contents ranging from 1.2 % to 4.1 %. All the data were taken at $T = 1.7$ K. For Eu contents above about 1.4 % the exchange-induced corrections to the spin-flip transitions are so large that in the low magnetic field range even the slope of $\hbar(\omega_L - \omega_S)$ versus B is changed. The calculation based on the mean-field approach yields the correct dependence both for holes (full curves) as well as for electrons with appropriate parameters (broken curves). The band and exchange parameters which are listed in tables 1-3 have been used in the calculations.

The influence of temperature on the spin-flip transition energies is shown in figure 23. It can be seen that at $T = 12$ K the exchange effects almost disappear, which means that the spin-flip energies behave as they do in a material having a higher energy gap than PbSe, as a consequence of the altered chemical composition.

The g-factors determined from the frequency differences, which correspond to the spin-flip energies versus

Table 3. Exchange parameters.

	T (K)	A (meV)	a_1 (meV)	B (meV)	b_1 (meV)
Mn content					
$x = 0.010$	1.8	-182 ± 15	-288 ± 15	-33 ± 10	27 ± 5
$x = 0.008$	1.8	-192 ± 15	-315 ± 15	-66 ± 10	55 ± 5
$x = 0.006$	1.8	-225 ± 15	-314 ± 15		50 ± 5
$x = 0.006$	3.5	-142 ± 15	-279 ± 15	-41 ± 10	50 ± 5
$x = 0.006$	4.4	-124 ± 15	-279 ± 15	-51 ± 10	51 ± 5
$x = 0.006$	12.0	-51 ± 15	-288 ± 15		59 ± 5
Eu content					
$x = 0.0142$	1.7	32 ± 3	30 ± 3	6.6 ± 1.6	7.5 ± 1.6
$x = 0.024$	1.7	24.4 ± 3	20 ± 3	6 ± 1.6	2.5 ± 1.6
$x = 0.024$	6.0	24 ± 3	18 ± 3	7.8 ± 1.6	0.9 ± 1.6
$x = 0.024$	12.0	22 ± 3	17.5 ± 3	9.7 ± 1.6	2.2 ± 1.6

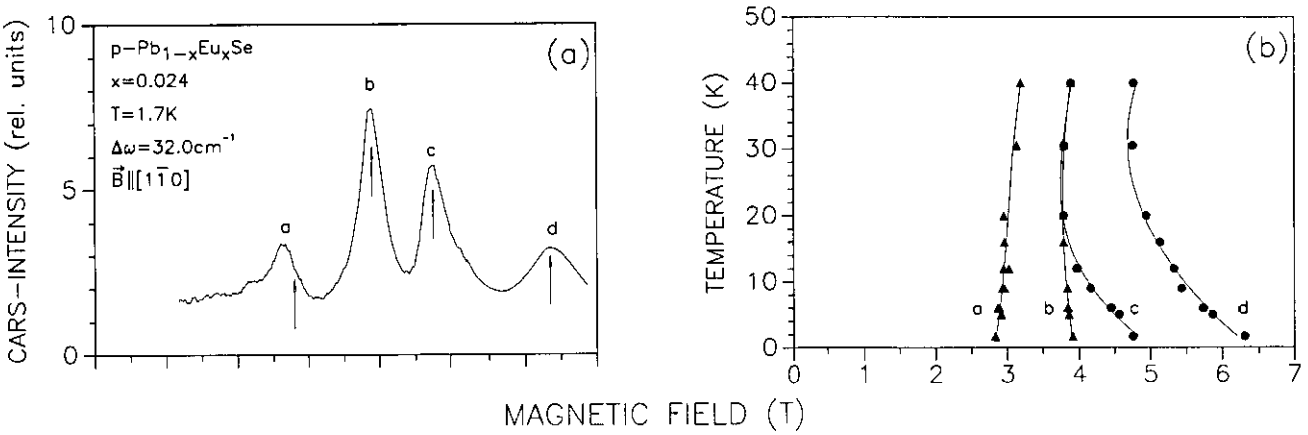

Figure 21. (*a*) CARS intensity versus magnetic field for $Pb_{1-x}Eu_xSe$ at a frequency difference $\omega_L - \omega_S = 32.0\ cm^{-1}$. Structures 'a' and 'b' are due to electron spin-flip resonances in the 35.26° and 90° valleys, respectively; 'c' and 'd' are due to holes. (*b*) Temperature dependences of resonant magnetic field for the two electron spin-flip resonances ('a', 'b') and the two hole resonances ('c', 'd'). (After Röthlein *et al* 1990.)

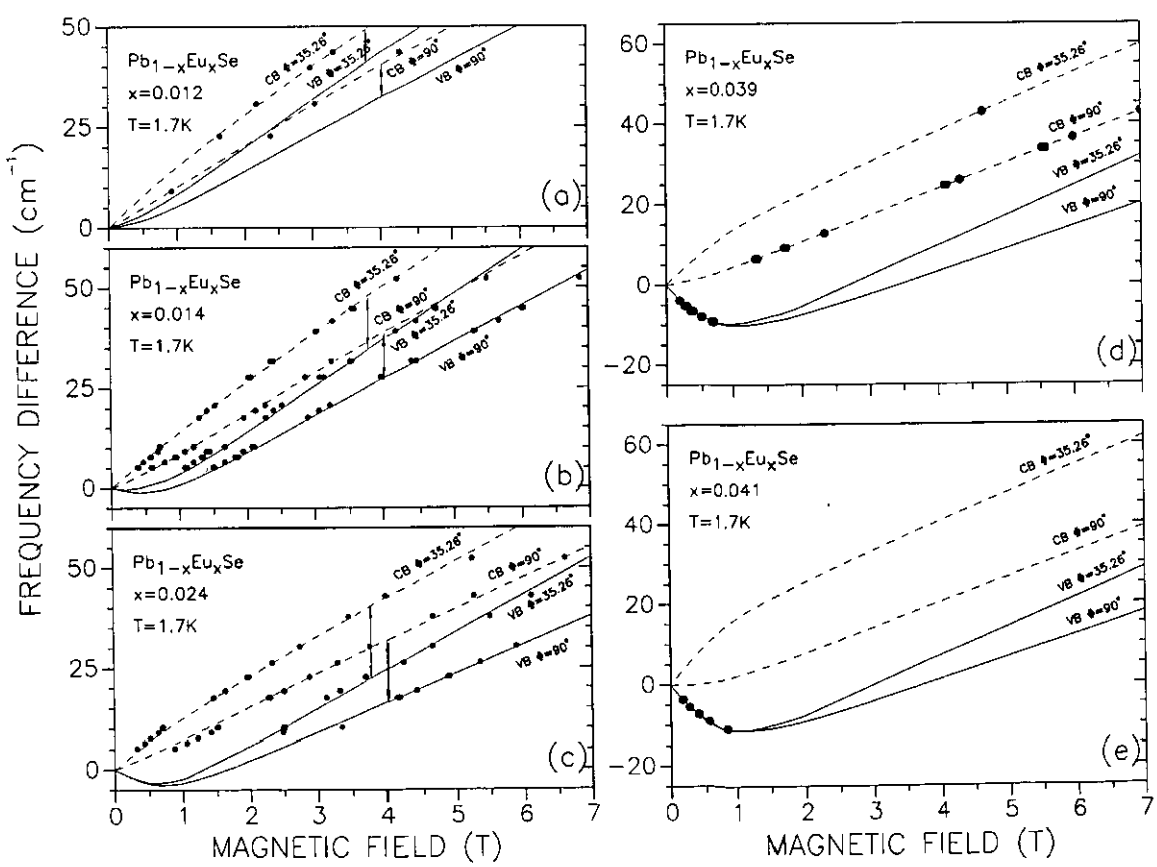

Figure 22. CARS measurements on $Pb_{1-x}Eu_xSe$ for five compositions x demonstrating the increasing influence of the exchange effects on the spin-flip transitions ($0^- \rightarrow 0^+$). Experimental data (●). Broken curves: calculated values for electrons (CB, $\phi = 35.26°$ and 90° valleys); full curves: calculated values for holes (VB, $\phi = 35.26°$ and 90° valleys).

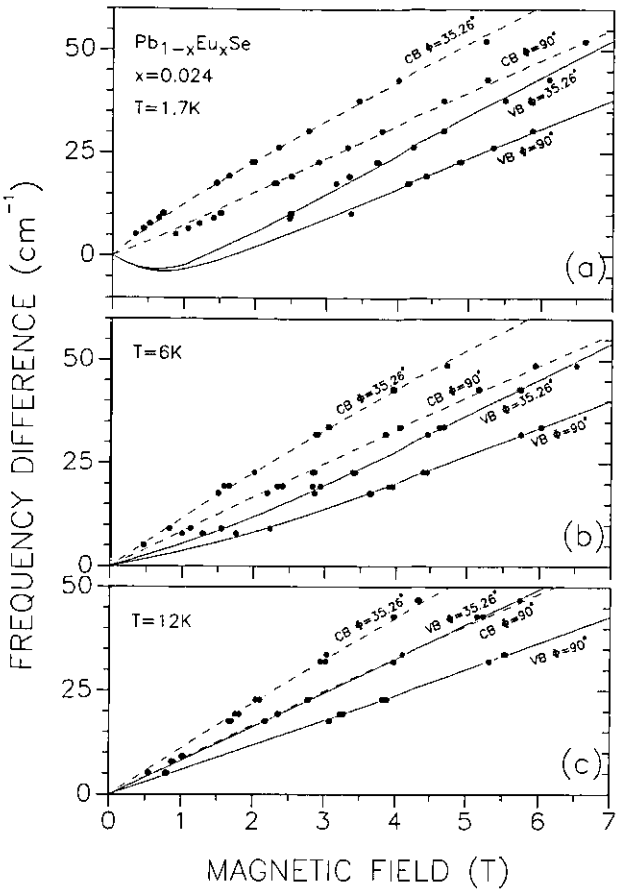

Figure 23. Spin-flip transition energies versus magnetic field for $Pb_{1-x}Eu_xSe$ at three temperatures, demonstrating the decreasing influence of exchange effects with increasing temperature. Experimental data (●). Calculated transitions for electrons (CB broken curves) and for holes (VB full curves).

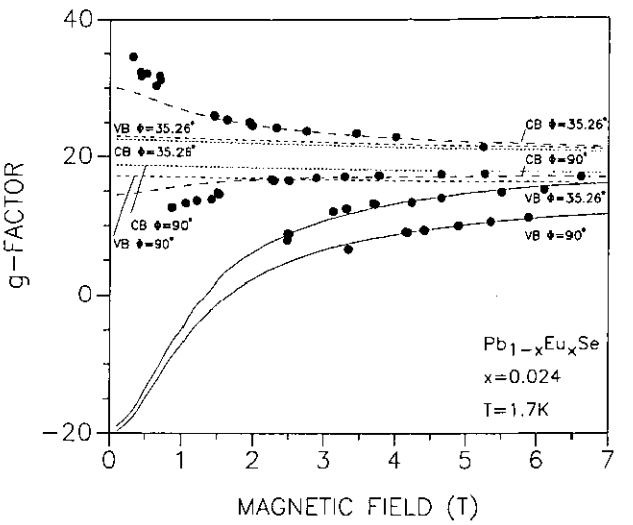

Figure 24. Magnetic field dependence of electron and hole g-factors in $Pb_{1-x}Eu_xSe$. Experimental data (●). Full curves: calculated values for holes (VB, $\phi = 35.26°$ and $\phi = 90°$). Broken curves: calculated values for electrons (CB, $\phi = 35.26°$ and $\phi = 90°$). Dotted curves: calculated magnetic field dependence of g-factors neglecting exchange effects. For low fields the exchange effects cause a sign change of hole g-factors which approach the values for saturated magnetization at high fields from below. The conduction band g-factor for $\phi = 35.26°$ valleys is *increased* at low fields, whereas for $\phi = 90°$ valleys the exchange effects *decrease* the g-factor.

B, are shown in figure 24 for PbEuSe, $x = 0.024$. In $Pb_{1-x}Eu_xSe$ the exchange interaction lowers the g-values for holes in both valleys. It even changes the sign of the g-factors for fields lower than 2 T. For the electrons, the exchange corrections increase the g-factor for the 35.26° valleys, but decreases that for the 90° valleys. The latter effect is possible because in IV–VI compounds we deal with *two* exchange parameters for the electrons and holes (see equations (33) and (41)).

The temperature dependence of the g-factors is summarized in figure 25. It shows a dramatic change of hole g-factors at low temperatures and a rather modest one for electrons. The negative contribution of the exchange interaction to the hole g-factors is so strong that it changes their signs to negative at low temperatures. As the temperature increases, its disorienting influence makes the influence of ion magnetization weaker and the hole g-factors become positive. The broken and dotted curves are calculated with the parameters of tables 1-3.

The dependence of the low-field g-factors on Eu concentration is shown in figure 26 for $B = 0.05$ T. The exchange interaction modifies the g-values from about +30 for holes in the 90° valleys and + 40 in the 35.26° valleys for PbSe to about − 90 at Eu contents of 7%. The exchange parameters are such that the two hole g-factors become identical for a concentration close to 2.5% where the corresponding lines for the 35.26° and 90° valleys cross each other. It is clear that $Pb_{1-x}Eu_xSe$ provides a large variety of tuning possibilities. These can be achieved with *magnetic field, temperature and composition.*

A similar presentation for $Pb_{1-x}Mn_xTe$ is shown in figure 27. Again, it is demonstrated that in both compounds the exchange-induced corrections are larger in the valence bands than in conduction band; however, their signs are different. In $Pb_{1-x}Mn_xTe$ the influence of

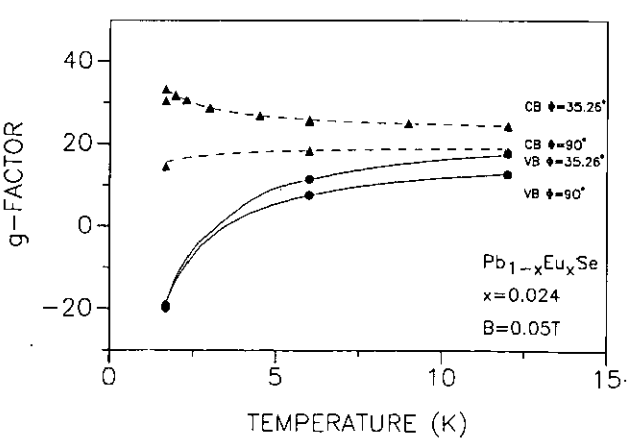

Figure 25. Temperature dependence of g-factors in $Pb_{1-x}Eu_xSe$ at $B = 0.05$ T. Experimental data for holes (●) and for electrons (▲). Full curves: calculated values for holes (VB, $\phi = 35.26°$ and $\phi = 90°$). Broken curves: the same for electrons. With increasing temperature the sign of the hole g-factors changes from negative to positive.

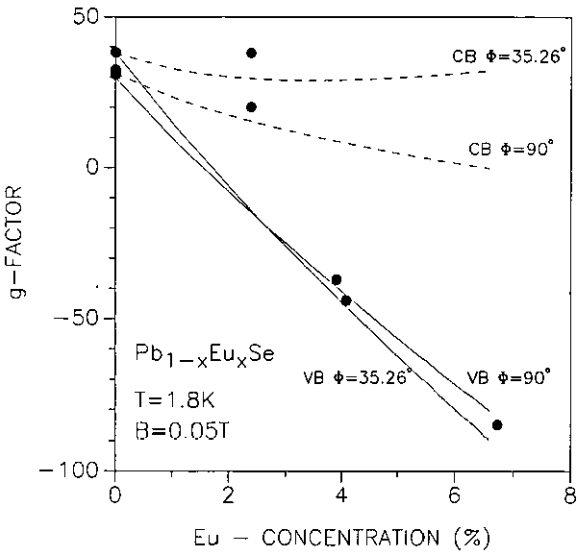

Figure 26. Dependence of electron and hole g-factors in $Pb_{1-x}Eu_xSe$ on Eu concentration. Experimental data (●). Full curves: calculated values for holes. Broken curves: calculated values for electrons. With increasing Eu content the hole g-factors change sign from positive to negative. The exchange effects also have a pronounced influence on the anisotropy of the g-factors and cause strong deviations from the values determined by band-structure anisotropies.

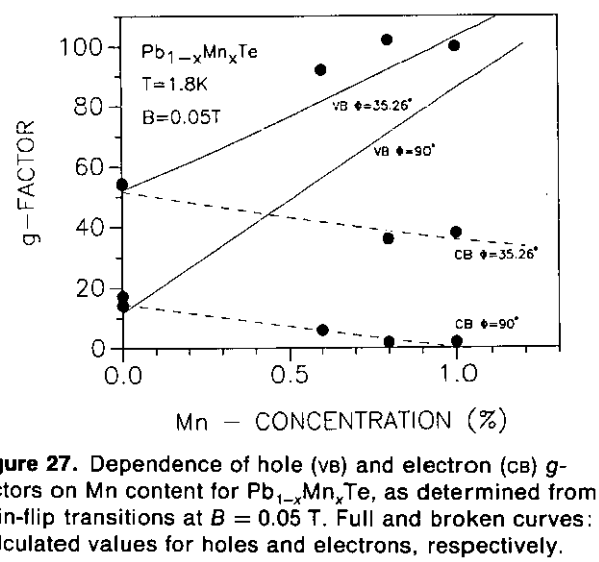

Figure 27. Dependence of hole (VB) and electron (CB) g-factors on Mn content for $Pb_{1-x}Mn_xTe$, as determined from spin-flip transitions at $B = 0.05$ T. Full and broken curves: calculated values for holes and electrons, respectively.

the exchange interaction with 1% Mn content is of the same order as that found in $Pb_{1-x}Eu_xSe$ $x \approx 6\%$ Eu content. Unfortunately, PbMnTe samples with a comparatively high Mn content and sufficiently high quality are not yet available.

4. Discussion

The semimagnetic IV-VI compounds bear some resemblance to the corresponding II-VI compounds. The partial substitution of the group IV(II) element by Mn causes an increase of the energy gap. The pseudobinary IV-VI compounds, with Eu partially replacing the group IV element, also have larger gaps than the binaries but also larger gaps in comparison with their pseudobinary Mn counterparts. The increase of the gap is the most important change of the band parameters. The two-band interband momentum matrix elements $P_\perp$ or $P_\parallel$ change only slightly with increasing Mn or Eu content. For the Mn or Eu concentration range investigated, the far-band parameters were taken to be constant and equal to the values which were obtained for the binary PbTe or PbSe compounds.

With increasing gap E_g, the latter assumptions become more and more questionable, since E_g might become a considerable fraction of the energy gaps to the more distant conduction or valence levels (see, e.g., Tomm *et al* 1990a, Goltsos *et al* 1985, 1986).

In the II-VI compounds, the Mn-Mn exchange is dominated by antiferromagnetic superexchange interactions, as was recently shown by Larson and Ehrenreich (1990). Anisotropic Mn-Mn exchange is only a small fraction of the isotropic superexchange. The exchange between the Mn ions in the IV-VIs which crystallize in the rock salt instead of zinc blende or wurtzite structure is also determined by superexchange (Gorska and Anderson 1988). However, so far no calculations of the d-d (or f-f) exchange constants exist for the lead compounds.

The exchange integrals for the free carrier and localized Mn^{2+} 3d electron interactions were determined both for II-VI and for IV-VI compounds. The behaviour of the exchange constants α (for the conduction band) and β (for the valence band in the II-VIs) turn out to be remarkably systematic. They are of opposite sign ($\beta < 0$, $\alpha > 0$), the exchange constant β for the valence band is always larger than that for the conduction band.

In the IV-VI compounds the conduction and valence band states are given by a linear combination of states which form a degenerate Kramers pair: the spin-orbit mixing parameters $\cos\theta^\pm$, $\sin\theta^\pm$ determine the contribution from the respective states (equation (33) in section 2). Correspondingly instead of one exchange constant for the conduction and a second one for the valence band states, there are in total *four* exchange constants for the IV-VI compounds. However, since the wavefunction admixtures are determined by the spin-orbit mixing parameters the two conduction and two valence band exchange integrals always appear in combination with spin-orbit mixing parameters $\cos\theta^\pm$, $\sin\theta^\pm$ (equations (32) and (33)).

The existence of two exchange parameters for the conduction band and two for the valence band has interesting consequences for the components of the g-tensors. The exchange effects not only change magnitude or sign of the components of the g-tensors but also the *anisotropy*. Such effects do not appear in the II-VI compounds which have their band extrema at the Γ point of the Brillouin zone.

In $Pb_{1-x}Eu_xSe$ the exchange effects change the sign of the g-factors of holes from positive to negative. Also their anisotropy is completely different from that determined

from the interband momentum matrix elements and the energy gaps. For Eu contents of about 6%, the absolute change of the g-factor is of the order of 100 as compared with the values without exchange. The existence of the two types of anisotropies, one determined by the band parameters the second by the exchange integrals, has a remarkable consequence: for a composition of about 3% and not too high magnetic fields (see figures 22 and 26) there is no anisotropy of the g-factors of holes; the g-factors for the 35.26° valleys and for the 90° valleys for $\boldsymbol{B} \| [1\bar{1}0]$ are identical.

Since from the fit to the experimental data one determines a_1, a_2, b_1 and b_2, which contain factors $\sin^2\theta^{\pm}$, $\cos^2\theta^{\pm}$ is it impossible to perform direct comparisons of the exchange integrals in II-VI and IV-VI semimagnetic compounds. Unfortunately, the uncertainty of the spin-orbit mixing parameters $\theta^{\pm}$ is too large to determine reliable values of the exchange integrals. From the fits one obtains the exchange parameters A and a_1 for the valence and B and b_1 for the conduction band. Comparing the numerical values for the Mn and Eu compounds (see table 3) it can be seen that both valence band parameters A and a_1 and one of the conduction band parameters (B) change sign if Eu replaces Mn. However, the parameter b_1 has the same sign in both compounds. This causes an increase of the g-factors of holes in valleys oriented by $\phi = 35.26°$ and 90° with respect to $\boldsymbol{B}$ in PbMnTe, and a decrease of both electron g-factors. In PbEuSe, in contrast, both hole g-factors are decreased, whereas the electron g-factors of the $\phi = 35.26°$ valleys are increased and those of the 90° valleys are decreased in comparison with the corresponding g-values determined by the gap and the interband momentum matrix elements (see figures 24 and 25). It is clear from these figures that the exchange effects have a profound influence on the g-factor anisotropy. The numerical values of the exchange parameters A, a_1, B, b_1 are smaller in the Eu compounds than in Mn compounds. For sufficiently high Eu contents ($x > 0.014$) the exchange effects cause a change of sign of hole g-factors from positive to negative.

The origin of the differences in the magnitude and sign of the four exchange parameters for Mn-based and Eu-based systems is difficult to assess. So far no photoemission or inverse photoemission data have been taken either on PbMnTe, PbMnSe samples or on PbEuSe. One can speculate that the 4f levels of Eu cause less hybridization with valence band states than the corresponding 3d levels of Mn. For all concentrations (Mn < 2%, Eu < 7%) the materials have still the electronic band structure of the host materials (PbTe or PbSe). The mass anisotropies of electrons and holes are not strongly changed with the addition of either Mn or Eu.

So far no impurity levels associated with Mn or Eu have been found within the energy gap. Recently Tomm *et al* (1990b) have found some evidence from luminescence involving recombination of excited electrons with states within the gap. However, no transitions were observed from Eu levels to the conduction band in absorption experiments so that one is led to the conclusion that in PbEuSe for compositions $x \leq 0.07$ the 4f states are still below the valence band edge.

Some of the IV-VI materials like $Pb_{1-x-y}Mn_xSn_yTe$ exhibit, for certain chemical compositions and hole concentrations ($p \approx 10^{20}\,cm^{-3}$), a ferromagnetic phase at low temperatures. The transition from the paramagnetic to the ferromagnetic phase is driven by RKKY interaction as shown originally by Story *et al* (1986) Recently de Jong *et al* (1990) and Galazka *et al* (1991) have quantitatively explained this phenomenon which involves subtle effects like the population of heavy-hole Σ bands with very high effective masses for sufficiently high hole concentrations. Both are decisive for the strength of the RKKY interaction. Unfortunately, the mobility in these samples $p \approx 10^{20}\,cm^{-3}$ is so low ($\approx 200\,cm^2\,V^{-1}\,s^{-1}$, Karczewski *et al* (1990)) that magneto-optical experiments are not possible.

First investigations of two-dimensional carriers confined in triangular or rectangular potential wells in semimagnetic IV-VI compounds have been reported. Kim and co-workers (1987) have measured cyclotron resonances in PbTe/PbEuSeTe and attempted to determine band offsets. Heyen *et al* (1989) have investigated time-resolved luminescence from PbTe/PbEuSeTe quantum wells. Pascher *et al* (1990) have studied by CARS spectroscopy g-factors in PbMnTe/PbTe multiquantum well structures. Krenn *et al* (1990) observed light-induced magnetization in these samples. The many-valley band structure causes complicated electric subband schemes for all growth orientations with the exception of [001]. Interesting effects, like penetration of carrier wavefunctions confined in diamagnetic wells into the barriers containing the magnetic ions, can be studied. Consequences of spatially modulated structures on the exchange effects present challenges for further experimental and theoretical work.

From the point of view of exchange interaction it would be of interest to study magnetic ions like Cr^{2+} or Fe^{2+} replacing Pb. Due to the non-zero orbital momentum of the free Fe or Cr ions, their ground states are split by the crystal field. Consequently, more complicated exchange phenomena occur. Apart from preliminary work on $Pb_{1-x}Cr_xTe$ (Akimov *et al* 1989) no investigations have been published to our knowledge.

The semimagnetic IV-VI compounds are of use as mid-infrared lasers, because of their direct energy gap. These lasers are tunable by external magnetic field, temperature and composition. In the lead compounds, the slope of dE_g/dT is positive and quite large in contrast to the II-VIs. Injection p-n lasers and quantum well lasers can be fabricated. PbEuTe or PbEuSe lasers are actually in use as sources for mid-infrared spectroscopy (Partin 1991, Tacke *et al* 1988, Roseman *et al* 1987, Ishida *et al* 1988).

Acknowledgments

This work was supported by Fonds zur Förderung der Wissenschaftlichen Forschung, Vienna, Austria and by

Deutsche Forschungsgemeinschaft, Bonn. We are grateful to Professor Peter Vogl, Munich, for helpful discussions concerning theoretical aspects of our subject and we thank Dr J Tomm, Berlin, for communicating results on luminescence data prior to publication and Professor T Dietl for a critical reading of the manuscript.

References

Adler M S, Hewes C R and Senturia S D 1973 *Phys. Rev.* B **7** 5186.
Akimov B A, Verteletzkii P V, Slomanov W P, Prasova I, Tananaseva O I and Shirokova N A 1989 *Fiz. Tekh. Poluprovod.* **23** 244
Anderson J R and Gorska M 1984 *Solid State Commun.* **52** 601
Anderson J R, Kido G, Nishina Y, Gorska M, Kowalczyk L and Golacki Z 1990 *Phys. Rev.* B **41** 1014
Baraff G A 1965 *Phys. Rev.* **137A** 842
Bauer G 1980 in *Narrow Gap Semiconductors, Physics and Applications* (*Lecture Notes in Physics 133*) ed W Zawadzki (Berlin: Springer) pp 427–46
—— 1983 in *Physics of Semiconducting Compounds* ed R R Galazka (Warsaw: Ossolineum) p 62
—— 1987 *Mater. Res. Soc. Symp. Proc.* **89** 107
—— 1991 in *Landau Level Spectroscopy* ed G Landwehr and E I Rashba (Amsterdam: North Holland) p 277
Bernick R L and Kleinman L 1970 *Solid State Commun.* **8** 569
Bir G L and Pikus G E 1974 *Symmetry and Strain-induced Effects in Semiconductors* (New York: Wiley) p 200
Braunstein G, Dresselhaus G, Heremans J and Partin D L 1987 *Phys. Rev.* B **35** 1979
Brueck S R J and Mooradian A 1973 *Opt. Commun.* **8** 263
Burkhard H, Bauer G and Zawadzki W 1979 *Phys. Rev.* B **19** 5149
Clemens H, Weilguni P C, Stromberger U and Bauer G 1989 *J. Vac. Sci. Technol.* A **7** 3197
Dalven R 1969 *Infrared Phys.* **9** 141
—— 1973 *Solid State Phys.* **28** 179 (New York: Academic)
de Jonge W J M and Swagten H J M 1991 *J. Magn. Magn. Mater.* in press
de Jonge W J M, Swagten H J M, Eltink S J E and Stoffels N M J 1990 *Semicond. Sci. Technol.* **5** S131
De Silets C S and Patel S K N 1973 *Appl. Phys. Lett.* **22** 543
Dimmock J O 1971 in *The Physics of Semimetals and Narrow Gap Semiconductors* ed D L Carter and R T Bate (Oxford: Pergamon) p 319
Elsinger G, Palmetshofer L and Lopez-Otero A 1983 *Nuovo Cimento* **2D** 1869
Evtuhov V 1962 *Phys. Rev.* **125** 1869
Furdyna J K 1988 *J. Appl. Phys.* **64** R29 and references therein
Furdyna J K and Kossut J (ed) 1988 in *Semiconductors and Semimetals* vol 25 (New York: Academic) pp 1–455
Gaj J A, Planel R and Fishman G 1979 *Solid State Commun.* **29** 435
Galazka R R and Kossut J 1980 in *Physics and Applications of Narrow Gap Semiconductors (Lecture Notes in Physics 133)* ed W Zawadzki (Berlin: Springer) p 245
Galazka R R, Spalek J, Lewicki A, Crooker B C, Karczewski G and Story T 1991 *Phys. Rev.* B **43** 11093
Goltsos W, Nakahara J, Nurmikko A V and Partin D L 1985 *Appl. Phys. Lett.* **46** 1173
Goltsos W C, Nurmikko A V and Partin D L 1986 *Solid State Commun.* **59** 183
Gorska M and Anderson J R 1988 *Phys. Rev.* B **38** 9120
Gorska M, Wojtowicz T and Knap W 1984 *Solid State Commun.* **51** 115
Hass K C 1991 in *Semimagnetic Semiconductors and Diluted Magnetic Semiconductors* ed M Averous and M Balkanski (New York: Plenum) p 59
Heremans J and Partin D L 1988 *Phys. Rev.* B **37** 6311
Heyen E T, Hagerott M, Nurmikko A V and Partin D L 1989 *Appl. Phys. Lett.* **54** 653
Ishida A, Nakahara N, Okamura T, Sase Y and Fujiyasu H 1988 *Appl. Phys. Lett.* **53** 274
Karczewski G and Kowalczyk L 1983 *Solid State Commun.* **48** 653
Karczewski G, Swierkowski L, Story T, Szczerbakow A, Niewodniezanska-Blinowska J and Bauer G 1990 *Semicond. Sci. Technol.* **5** 1115
Karczewski G and von Ortenberg M 1984 in *Proc. 17th Int. Conf. on the Physics of Semiconductors, San Francisco* ed J D Chadi and W A Harrison (New York: Springer) p 1435
Karczewski G, von Ortenberg M, Wilamowski Z, Dobrowolski W and Niedwodniczanska-Zawadzka J 1985 *Solid State Commun.* **55** 249
Kim L S, Drew H D, Doezema R E, Heremans J P and Partin D L 1987 *Phys. Rev.* B **35** 2521
Kowalczyk L 1991 *Semicond. Sci. Technol.* **6** 115
Krenn H, Kaltenegger K, Frank N, Bauer G, Kriechbaum M and Pascher H 1990 in *Proc. 20th Int. Conf. on the Physics of Semiconductors* ed E M Anastassakis and J D Joannopoulos (Singapore: World Scientific) p 1162
Lambrecht A, Herres N, Spranger B, Kuhn S, Böttner H, Tacke M and Evers J 1991 *J. Cryst. Growth* **108** 301
Larson B E and Ehrenreich H 1990 *J. Appl. Phys.* **67** 5084
Lax B and Mavroides J G 1960 in *Solid State Physics* vol II ed F Seitz and D Turnbull (New York: Academic) p 261
Martinez G, Schlüter M and Cohen M L 1975 *Phys. Rev.* B **11** 651
McKnight S W and Drew H D 1980 *Phys. Rev.* B **21** 3447
Mitchell D L and Wallis R F 1966 *Phys. Rev.* **151** 581
Niedwodniczanska-Zawadzka J, Elsinger J G, Palmetshofer L, Lopez-Otero A, Fantner E J, Bauer G and Zawadzki W 1983 *Physica C + C* **117 and 118B** 458
Niedwodniczanska-Zawadzka J, Kossut J, Sandauer A and Dobrowolski W 1982 *Lecture Notes in Physics* **152** (Berlin: Springer) p 326
Partin D L 1988 *IEEE J. Quantum Electron.* **24** 1716
—— 1991 in *Semiconductors and Semimetals* vol 33 ed T P Pearsall (New York: Academic) p 311
Pascher H 1984 *Appl. Phys.* B **34** 107
—— 1990 *Semicond. Sci. Technol.* **5** S141
Pascher H and Bauer G 1987 in *High Magnetic Fields in Semiconductor Physics* ed G Landwehr (Berlin: Springer) p 400
Pascher H, Bauer G and Grisar R 1988a *Phys. Rev.* B **38** 3383
Pascher H, Fantner E J, Bauer G, Zawadzki W and von Ortenberg M 1983 *Solid State Commun.* **48** 461
Pascher H, Röthlein P, Bauer G and Palmetshofer L 1987 *Phys. Rev.* B **36** 9395
Pascher H, Röthlein P, Bauer G and von Ortenberg M 1989 *Phys. Rev.* B **40** 10469
Pascher H, Röthlein P, Kriechbaum M, Frank N and Bauer G 1990 *Superlatt. Microstruct.* **8** 69
Pascher H, Röthlein P, Roschger I and Bauer G 1988b in *Proc. 19th Int. Conf. on the Physics of Semiconductors* ed W Zawadzki (Warsaw: Institute of Physics, Polish Academy of Sciences) p 1535
Pascher H, Röthlein P, Roschger I and Tacke M 1988c in *Proc. 19th Int. Conf. on the Physics of Semiconductors* ed W Zawadzki (Warsaw: Institute of Physics, Polish Academy of Sciences) p 1591
Patel C K N, Slusher R E and Fleury P A 1966 *Phys. Rev. Lett.* **17** 1011
Pfeffer P and Zawadzki W 1990 *Phys. Rev.* B **41** 1561

Ravich Y I, Efimova B A and Smirnov I A 1970 *Semiconducting Lead Chalcogenides* (New York: Plenum)
Roseman R, Katzir A, Norton P, Bachem K-H and Preier H M 1987 *IEEE J. Quantum Electron.* **23** 94
Röthlein P, Pascher H, Bauer G and Tacke M 1990 *Semicond. Sci. Technol.* **5** S147
Schaber M Ch and Doezema R E 1979 *Phys. Rev.* B **20** 5257
Story T, Galazka R R, Franke R B and Wolff P A 1986 *Phys. Rev. Lett.* **56** 777
Story T, Karczewski G, Swierkowski L, Gorska M and Galazka R R 1990 *Semicond. Sci. Technol.* **5** S138
Tacke M, Spranger B, Lambrecht A, Norton P R and Böttner H 1988 *Appl. Phys. Lett.* **53** 2260
Tomm J W, Hermann K H, Böttner H, Tacke M and Lambrecht A 1990b *Phys. Status Solidi* a **11a** 711
Tomm J W, Herrman K H and Yunovich A E 1990a *Phys. Status Solidi* a **122** 11
Valeiko M V, Zasavitskii I I, Matsonashvili B N and Rukhadze Z A 1991 *Superlatt. Microstruct.* in press
von Ortenberg M 1980 in *Intrared and Millimeter Waves* vol III ed K Button (New York: Academic) p 275
von Ortenberg M, Bauer G and Elsinger G 1985 *Proc. Int. Conf. Millimeter Waves*, Marseille p 53
Wolff P A and Pearson G A 1966 *Phys. Rev. Lett.* **17** 1015
Zasavitskii I I, Kowalczyk L, Matsonashvili B N and Sazonov A V 1988 *Fiz. Tekh. Poluprovodn.* **22** 2188 (Engl. transl. *Sov. Phys.–Semicond.* **22** 1388)
Zasavitskii I I and Sazonov A V 1988 *Fiz. Tverd. Tela* **30** 1669 (Engl. transl. *Sov. Phys.–Solid State* **30** 962)
Zeiger H J and Pratt G W 1973 *Magnetic Interactions in Solids* (Oxford: Clarendon)